INSTITUTO POLITÉCNICO DE LISBOA

Instituto Superior de Engenharia de Lisboa

Escola Superior de Tecnologia da Saúde de Lisboa

Nanostructured films of graphene for controlled ocular drug delivery

Helena Isabel Costa Morais

Trabalho Final de Mestrado para obtenção do grau de
Mestre em Engenharia Biomédica

Orientadores:
Dr.ª Quirina Alexandra Tavares Ferreira (Instituto de Telecomunicações)
Dr.ª Ana Maria de Matos Charas (Instituto de Telecomunicações)
Prof. Dr. Manuel José de Matos (ISEL)

Membro do Júri

Presidente: Dr.ª Cecília R. C. Calado (ISEL)

Orientador: Dr.ª Quirina Alexandra Tavares Ferreira (Instituto de Telecomunicações)

Arguente: Prof.ª Dr.ª Maria de Fátima Guerreiro da Silva Campos Raposo (Faculdade de Ciências e Tecnologia, Universidade Nova de Lisboa)

Dezembro 2017

INSTITUTO POLITÉCNICO DE LISBOA

Instituto Superior de Engenharia de Lisboa
Escola Superior de Tecnologia da Saúde de Lisboa

Nanostructured films of graphene for controlled ocular drug delivery

Helena Isabel Costa Morais

Thesis to obtain the Master of Science Degree in
Biomedical Engineering

Supervisors:
Dr. Quirina Alexandra Tavares Ferreira (Instituto de Telecomunicações)
Dr. Ana Maria de Matos Charas (Instituto de Telecomunicações)
Prof. Dr. Manuel José de Matos (ISEL)

Examination Committee

Chairperson: Dr. Cecília R. C. Calado (ISEL)

Supervisor: Dr. Quirina Alexandra Tavares Ferreira (Instituto de Telecomunicações)

Member of the Committee: Prof. Dr. Maria de Fátima Guerreiro da Silva Campos Raposo
(Faculdade de Ciências e Tecnologia, Universidade Nova de Lisboa)

December 2017

“The secret of getting ahead is getting started”

Mark Twain

Agradecimentos

Terminada esta etapa gostaria de agradecer à minha orientadora, Doutora Quirina Alexandra Tavares Ferreira, por todos os conhecimentos passados, pelo tempo disponibilizado, e pelo apoio prestado, foi verdadeiramente importante e crucial para o sucesso desta Tese.

À minha co-orientadora Doutora Ana Maria de Matos Charas, também agradeço por todos os conhecimentos transmitidos, sempre disponível quando necessário, sabendo sempre transmitir palavras de encorajamento.

Agradeço também às colegas, com quem partilhei grande parte do meu tempo no laboratório, Cristiana Costa, Mónica Machado e Mariana Velho, estando sempre disponíveis para me ajudar e tornando o ambiente no laboratório mais agradável e entusiasmante.

Não poderia deixar de agradecer aos meus amigos de longa data, Maria Inês Curado e João Costa que sempre me apoiaram e estiveram presentes nos bons e maus momentos, que sempre me deram motivação para continuar, com boa disposição, e companheirismo sem eles todo este caminho seria sem dúvida mais árduo. Um agradecimento especial aos meus colegas e amigos que conheci neste mestrado, Marta Neves, Daniela Teixeira e Ricardo Pimenta, pelos bons momentos vividos, cheios de boas memórias, que para sempre irei recordar com carinho.

Ao David Neto, meu namorado e companheiro, agradeço especialmente pelo afeto, carinho e boa disposição transmitidos diariamente, pela força e encorajamento dados. Esteve sempre presente para me animar e apoiar, não só neste percurso, mas em todos os grandes marcos da minha vida.

Por último guardo o meu agradecimento mais valioso para meus os pais, Maria Helena Morais e Abílio Morais e para o meu irmão, Ricardo Morais, por todo o apoio incondicional e carinho. Por acreditarem sempre em mim, estando sempre presentes na minha vida. A eles dedico todo este trabalho.

Nanostructured films of graphene for controlled ocular drug delivery

Helena Isabel Costa Morais

2017

This thesis was fully performed at Organic Electronics Group at Instituto de Telecomunicações, under supervision of Dr. Quirina Ferreira and Dr. Ana Charas in the scope of the Master Thesis in Biomedical Engineering of ISEL - Instituto Superior de Engenharia de Lisboa and ESTeSL- Escola Superior de Tecnologia da Saúde de Lisboa.

Resumo

O glaucoma é uma doença degenerativa ocular que prejudica o nervo ótico do olho, o que leva a um aumento da pressão intraocular (IOP) e pode resultar em perda total e irreversível de visão. O tratamento disponível até há data baseia-se na administração do fármaco brimonidina através de gotas oculares de forma a diminuir a IOP. Porém, a adesão dos pacientes ao tratamento de administração de gotas é, em geral, baixa, o que conduz ao agravamento da doença. O objetivo desta tese foi desenvolver um filme biocompatível que possa servir de revestimento para um dispositivo intraocular, que permita a libertação da brimonidina de forma programada, autónoma e *in situ*. Os filmes foram preparados pela técnica camada-sobre-camada e são compostos por monocamadas de brimonidina encapsulada em 2-hidroxipropil-ß-ciclodextrina intercaladas por camadas que atrasam a libertação do fármaco e que se designam por camadas barreira. Estas últimas são compostas por um polímero hidrossolúvel (PBAE) e por bicamadas de óxido de grafeno (GO) compostas por grafeno positivo funcionalizado com grupos amina protonados ($GONH_3^+$) e por grafeno negativo funcionalizado com grupos carboxílicos desprotonados (COO^-). Foram preparados três tipos de filmes, a diferença entre os dois primeiros filmes foi a alteração da ordem das camadas de GO de forma a verificar a sua interação com a camada de brimonidina e o terceiro filme apenas contém um tipo de camada barreira compostas por GO, retirando-se o polímero hidrossolúvel PBAE, de forma a verificar a sua influencia na cinética de libertação da brimonidina. O crescimento dos filmes foi monitorizado por espectroscopia de absorção no ultravioleta e visível (UV-Vis) e microscopia de força atómica (AFM) e a cinética de libertação do fármaco foi controlada por UV-Vis e por cromatografia líquida de alta eficiência (HPLC). Os resultados mostraram que os filmes são estáveis e que a libertação do fármaco pode ser controlada pela presença do polímero hidrossolúvel e do óxido de grafeno. Nomeadamente, a presença de GO atrasa a libertação de brimonidina por vários dias dependendo do número de camadas existentes no filme.

Palavras-chave: Glaucoma, camada-sobre-camada, libertação controlada de fármacos, brimonidina, 2-hidroxipropil-β-ciclodextrina e óxido de grafeno.

Abstract

Glaucoma is an ocular degenerative disease that damages the eye's topic nerve, this leading to an intraocular pressure (IOP) increase which can result in a total and irreversible loss of vision. The available treatment at the moment is based on brimonidine administration which allows the decrease of IOP, by administration of ocular drops, in order to decrease IOP. However, adherence of patients to the treatment of droplet administration is generally low, which leads to the worsening of the disease. The aim of this thesis was to develop a biocompatible film that can serve as coating for an intraocular device, allowing the brimonidine release to be programmed, autonomous and *in situ.* The films were prepared by layer-on-layer technique and were composed of brimonidine monolayers encapsulated in 2-hydroxypropyl-β-cyclodextrin interspersed by layers that delay drug release and are referred to as barrier layers. These layers are composed of a water soluble polymer (PBAE) and graphene oxide (GO) composites composed of graphene positive functionalized with protonated amine groups ($GONH3^{+}$) and negative graphene functionalized with deprotonated carboxylic groups (COO^{-}). Three types of films were prepared, the difference between the first two films was the change in the order of the GO layers in order to verify their interaction with the brimonidine layer and the third film only contains a type of barrier layer composed of GO, by removing the water soluble polymer PBAE, in order to verify its influence on the brimonidine release kinetics. The film growth was monitorized by ultraviolet-visible absorption spectroscopy (UV-Vis) and atomic force microscopy (AFM) and the drug release kinetics was followed by UV-Vis absorption spectroscopy and high performance liquid chromatography (HPLC). The results have shown that the obtained films are stable and the drug release can be controlled by the presence of the hydrossoluble polymer and the graphene oxide. Notably, the presence of GO layers delays the brimonidine release for several days depending on the number of layers in the film.

Keywords: Glaucoma, layer-by-layer, controlled drug delivery, brimonidine, 2-hydroxypropyl-β-cyclodextrin and graphene oxide.

Contents

List of tables

List of figures

Nomenclature

POAG	Primary open angle glaucoma
OAG	Open angle glaucoma
IOP	Intraocular pressure
NDA	New Drug Application
CD	Cyclodextrin
PAH	Poly(allylamine hydrochloride)
PSS	Poly(styrene sulfonate)
PAA	Poly(acrylic acid)
GO	Graphene oxide
GO^+	Positively charged graphene oxide
GO^-	Negatively charged graphene oxide
2-Hydroxypropyl-β-cyclodextrin	HP-ß-CD+Brim
LGN	Lateral geniculate nucleus
RGC	Retinal ganglion cell
SC	Superior colliculus
DD	Drug delivery
LbL	Layer-by- layer
PBAE	Poly(ß-amino ester)
M_W	Weight-average molecular weight
PBS	Phosphate-buffered saline
UV-VIS	Ultraviolet-visible absorption spectroscopy
AFM	Atomic Force Microscopy
NMR	Neutral Magnetic Resonance
IR	Infrared
HPLC	High Performance Liquid Chromatography
LC	Liquid Chromatography

Chapter 1 - Introduction

1.Introduction

1.1 Glaucoma and drug delivery systems for ocular devices

1.1.1 Glaucoma

According to the World Health Organization, glaucoma is one of the diseases that causes total blindness. It is estimated that the number of persons affected by glaucoma is about 4.5 million and that globally this disease is the second leading cause of blindness (6). Also, it is predicted that by 2020, close to 4 millions of Americans will have glaucoma from which ca. 50% will be undiagnosed and approximately 120,000 individuals will develop blindness (7) (8). Glaucoma is characterized by an optic neuropathy that leads to progressive vision loss and in more extreme cases causes blindness. It is a chronic and degenerative neuropathy that can be distinguished by the characteristic appearance of the optic nerve (9) (10) (11). It is characterized by elevated intraocular pressure; development of optic nerve atrophy, and loss of the peripheral field of vision, culminating in the so-called “impairing central vision” (Figure 1) (12). The risk factors are mostly age, gender, race and genetics, but the major cause is elevated intraocular pressure (IOP) (10)(13).

Figure 1 - Progression of vision loss of a person with open angle glaucoma.
(from http://www.floridaeyespecialistinstitute.com/services/glaucoma/ in 2016.11.08)

The IOP can be determined by the rate of the aqueous outflow and the episcleral venous pressure (14). The available treatment so far is mostly pharmacologically and surgically that allows for stabilizing the IOP with eye drops composed of alpha2-

adrenergic agonists (i.e. Brimonidine). The surgery contributes to create a new opening which helps the fluid to leave the eye, and consequently lowers the IOP. However, the patient needs to administrate eye drops on a daily basis, this representing the major problem on the present treatment of glaucoma, since a significant lack of patients´ adherence to the daily topical treatment has been verified (patients' do not renew their prescriptions resulting in regularly missing doses) (7)(13).

A schematic representation of the effect of IOP in the human eye, can be seen in figure 2. The eye affected by glaucoma shows aqueous humour that is not correctly drained, leading to an increase of pressure.

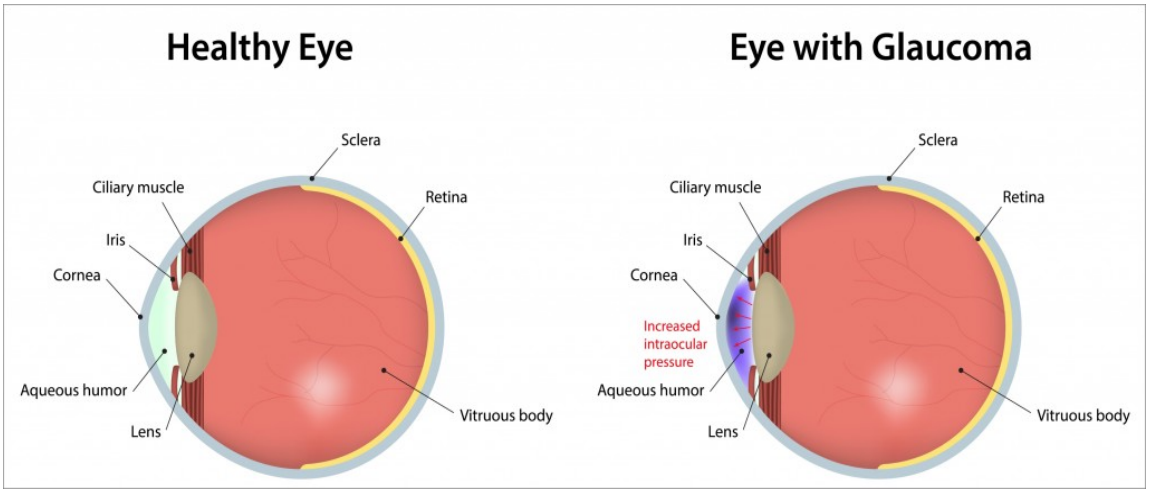

Figure 2 - Schematic representation of a normal eye comparing with an eye with glaucoma. Adapted from (60).

Figure 3 represents a diagram showing the structures that are affected by high IOP and the effects of the glaucoma at a high developing state (vision loss).

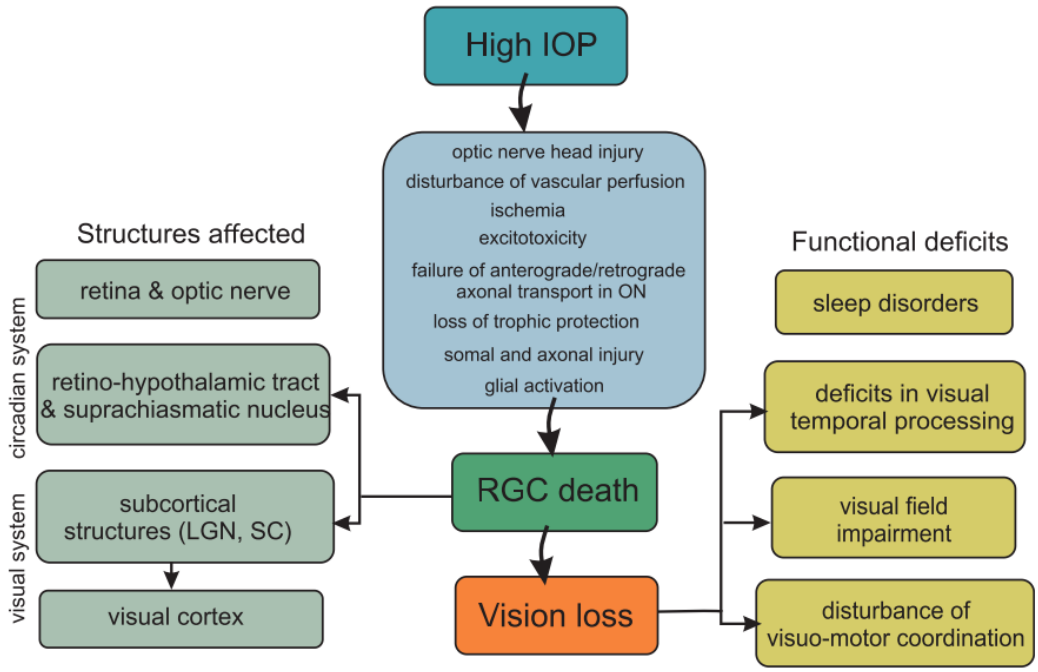

Figure 3 - Most common factors of glaucoma triggered by elevated intraocular pressure and its structural and functional consequences (12).

Thus, considering the poor IOP control provided by the current treatments, it is therefore imperative to develop a method of drug delivery which does not depend on the patient compliance.

1.1.2 Drug Delivery

Drug delivery (DD) refers to a formulation or a device that enables the insertion and transport of a therapeutic substance in the body. Currently great efforts have been dedicated to the development of targeted and controlled DD, by accurately controlling the rate, time, and place of release of drugs in the body. An ideal DD system should present the following features (15):

- It should increase the bioavailability of the drug;
- It should provide for controlled DD;

- It should transport the drug intact to the site of action while avoiding the non-diseased host tissues;
- The product should be stable and the delivery should be maintained under various physiological variables;
- Its administration to the patients should be easy;
- It should be safe and reliable;
- It should be cost-effective.

A DD system can be characterized by the following properties:

- Physical state - the dosage forms can be administrated in gaseous form (e.g. anaesthetic), liquid (e.g. solutions, emulsions, suspensions), semi-solid (e.g. cream, ointments, gel and pasts) and solid dosage (e.g. powders, granules, tablets and capsules). Some cases have more than one type of physical state. In this thesis, the developed DD system has a solid form.
- Route of administration - drugs can be administrated directly into the body, through injection or infusion. Depending on the site of administration, it is possible to differentiate between intravenous, intramuscular, subcutaneous, intradermal and intraperitoneal. In this thesis, the developed DD system to release the drug is *in situ*.
- Mechanism of drug release - the drug release process can be classified as an immediate release, where the drug is released immediately after administration, and a modified release, that occurs after administration or to a specific target in the body. This modified release can be classified as delayed release, where the drug is released only at some point after the initial administration or it could be an extended release, i.e. the release is prolonged to reduce the dosing frequency. In this thesis, the developed DD systems function accordingly to a modified release and the two different kinds were developed: delayed and extended release (16).

1.1.3 Time-controlled drug delivery

The control of time and dosage of the therapeutic drugs is crucial to improve patient care but a very precise control of the DD mechanism is required to allow for enlarging the period of release from a few hours to long periods, as months, which are generally convenient.

A time-controlled DD system should provide a sequential release of the drug improving its delivery and its availability at the target organ/tissue. These systems can be prepared as multilayer films which can coat devices placed either inside or on the surface of the body (17).

A recent work developed by Paula T. Hammond *et al*. (17) demonstrated a controlled DD system, consisting of a multilayer film which included graphene oxide as a barrier layer to delay the drug release. In such study, the number of graphene oxide (GO) layers was found to be proportional to the time delay of the drug and the extend the drug release from 30 to 90 days by varying the number of bilayers of functionalized GO (17). Such barrier layers to delay the drugs release act as grouped films in order to regulate the drug release and also regulate interlayer diffusion. By alternating layers of polyelectrolytes exhibiting linear growth, within the film, such as of poly(allylamine hydrochloride) (PAH), poly(acrylic acid) (PAA), poly(styrene sulfonate) (PSS) and Poly(ß-amino esters) (PBAE), it is also possible to accomplish the release of multiple drug types in an ordered and temporally controlled manner (17) (18).

1.1.4 Drug delivery layer-by-layer films for biomedical applications

The layer-by-layer (LbL) assembly was introduced for the first time by Decher, in 1992 (19), as an assembly technique based on complementary chemical interactions. This technique involves the alternating adsorption of different charged molecular species from buffered aqueous media to build a film. It provides an alternative approach to traditional polymer-based delivery systems, since the polymer delivery matrix is built one layer at a time and the drug of choice is inserted in alternated layers (17). LbL assembly is a cyclical process in which a charged material is adsorbed onto a substrate, and after washing, an oppositely charged material is adsorbed on top of the first layer. Figure 4 depicts a schematic representation of the process (20).

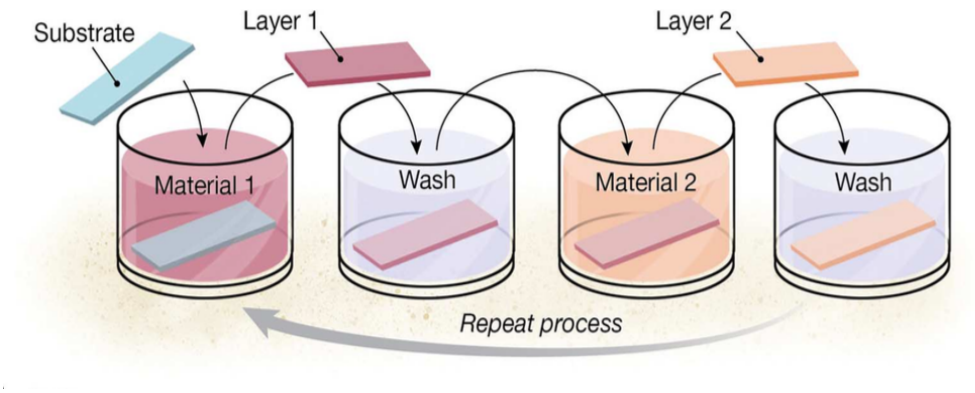

Figure 4 - Schematic representation of the LbL method. Adapted from (20).

The LbL assembly technique is versatile, allowing the incorporation of a broad range of functional polymers, biomacromolecules and other charged species (17) (19).

Besides simplicity, the LbL method offers several advantages, such as: allows for a precise control of the coating properties; it is environmentally friendly; it is low-cost; it's versatility for coating a wide range of surfaces; provides homogeneous films with controlled thickness and allows the incorporation and controlled release of biomolecles/drugs (21) (20). The process of LbL allows for depositing not only water-soluble linear charged polymers, but also viruses, proteins, dyes, metal oxides, amphiphilic molecules, etc (21). Remarkably, the LbL technique has been already used for functionalizing scaffolds and medical devices for different applications. In the medical field, this method has been mostly used to prepare DD vehicles, more specifically multilayer coatings fabricated on the top of a nanoparticle core. The core is then removed in order to obtain an empty shell that can be loaded and functionalized with different biomolecules or drugs (21). The interdiffusion and mixing of polyionic species during assembly can limit the ability to control the film architecture for many biomedical applications; thus, such multilayer films release biologic drugs with little or no control of drug sequence (17).

The LbL method used in this thesis to prepare the DD films allowed a sequential adsorption of several layers immersing a charged substrate in a different polymer solution. After each immersion in a polymer solution, the sample should be washed, in order to remove the physically adsorbed particles, ensuring that the remaining layers are homogeneous (20). This procedure can be repeated as many times as necessary until the desired number of layers is achieved.

1.1.5 Brimonidine

Brimonidine (see figure 5 for molecular formula) is an alpha2-adrenergic agonist and one of the most used anti-glaucoma drugs. Moreover, several studies have suggested that brimonidine may have additional neuroprotective effects on the optic nerve (12).

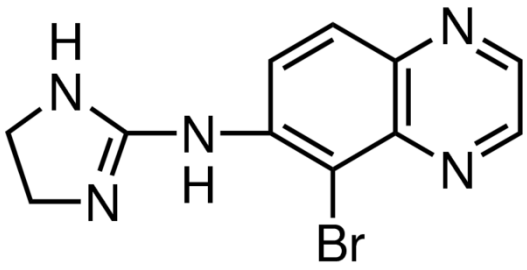

Figure 5 - Chemical structure of brimonidine.

Brimonidine is rapidly absorbed and well distributed in the eye and its systemic metabolism is extensive, in humans, first it is metabolized primarily by the liver. The urinary excretion is the major route of elimination of the brimonidine and its metabolites, (approximately 87% of an orally-administered dose are eliminated within 120h, being 74% through urine). Topically administered daily ophthalmic brimonidine is indicated for IOP reduction in patients with ocular hypertension and/or open angle glaucoma (OAG). Generally, brimonidine is administered as topical eye drops between 2 to 3 times per day (7) (8). Brimonidine has been evaluated extensively for ocular and systemic toxicity in several animal models, as required to support a new drug application (NDA). Ocular (0.08-0.8%, twice daily) and systemic (0.1-2.5 mg/kg/day by oral/diet) administration for up to one year produced no organ toxicity, despite plasma levels of 4 to 118 times the systemic exposure in humans following ocular administration with 0.2%. Studies have shown no oncogenic or teratogenic activity, nor adverse effects on fertility and reproduction. These results indicate that brimonidine is nontoxic and safe. In addition, several clinical studies have determined that brimonidine has ocular hypotensive efficacy in a lower concentration than clonidine (first relatively selective alpha2-adrenergic agonist) or apraclonidine (8) (22).

1.1.6 Graphene oxide nanosheets

Graphene, a two-dimensional nanomaterial consisting of sp^2 hybridized carbon atoms, is a basic building block for graphitic materials with other dimensionalities. Given its large specific surface area, good chemical stability and other excellent properties (in particular, electric properties) graphene holds great promise in different areas. GO refers to graphene functionalized with oxygen in the form of ether, hydroxyl, carboxyl, and epoxy. GO can be used to create barrier layers in multilayer films by trapping molecules of interest for controlled release (23) (17) (24) (17).

One study performed by Paula T. Hammond et al. (17) showed films fabricated with the LbL assembly technique, with GO with charged functional groups and PBAE, which delay the drug release from less than one hour to 30 or even 90 days, depending on the number of bilayers of functionalized GO in the LbL architecture (17). GO can form stable dispersions in water because of its high oxygen-containing groups. Conversely, if the oxygen functionality is removed by chemical reduction to yield graphene, this aggregates and can precipitate due to the π-π* interactions between the conjugated nanosheets of graphene (25).

Regarding toxicity issues, GO in doses of less than 20 μg/mL is toxic to human fibroblast cells, in doses higher than 50 μg/mL, some cytotoxicity arises, such as decreasing cell adhesion, inducing cell apoptosis, entering lysosomes, mitochondrion, endoplasm, and cell nucleus. The possible mechanism of GO's cytotoxicity is the following: the GO in the medium bind with the surface of human cells, providing a stimuli signal to the cells. The signal is transduced inside the cells and the nucleus leading to down-regulation of adhesion-associated genes and corresponding adhesive proteins. This results in a decrease in cell adhesion and cause cells to detach, float, and shrink in size. GO enters into the cytoplasm by endocytosis pathway, mainly located in the lysosomes, mitochondrion, endoplasm and cell nucleus, where it may disturb the course of cell energy metabolism and gene transcription and translation, and even result in cell apoptosis or death (26) (17).

1.1.7 Poly (ß-amino esters)

Poly(ß-amino esters) (PBAE) (see figure 6 for chemical structure) are a class of biodegradable polymers (27), which are degradable by hydrolysis. PBAE is produced through Michael addition polymerization of acrylate and amine monomers (28).

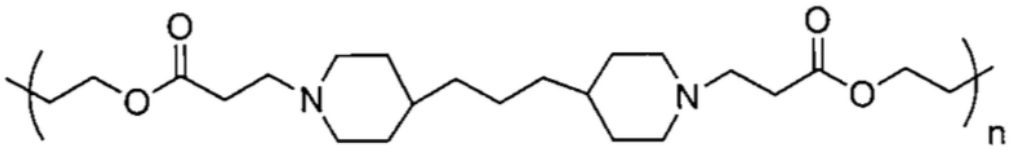

Figure 6 - Chemical structure of PBAE. Figure adapted from (27).

These class of hydrolytically biodegradable polymers can be easily obtained in large scale to make a large library of structurally diverse materials. Their hydrolysis occurs on the time scale of several hours to a few days, and is largely affected by the polymer structure as well as the cellular conditions. Also, some studies have shown that the PBAE degrades faster at pH 7 than at pH 5. (29)(30) PBAE shows low cytotoxicity; studies described in references (30) (31) show the biocompatibility and biodegradability of this compound. Additionally, it was demonstrated that and NIH 3T3 fibroblast cells incubated with PBAE remain 100% viable, for concentrations of polymer up to 100 µg/mL (27). Considering such advantageous properties, in particular the fact that its hydrolysis can take from several hours to a few days, the polymer (PBAE) was used in order to create a DD system with programmable and sequential release (29)(17).

1.1.8 Cyclodextrin

Cyclodextrins (CD) are cyclic oligosaccharides, the main natural CD (α, ß and γ) are constituted of 6, 7 and 8 glucopyranose units connected by α(1,4)-linkages, respectively, but larger ones have been also isolated (32). CDs have a hydrophobic cavity able to encapsulate multiple molecules, due to their capability to form noncovalent inclusion complexes with a large variety of guest molecules (33) (34). These characteristics have determined their applicability in different fields. CDs have mainly been used in the pharma area, as DD systems to improve the solubility of drugs. Furthermore, the properties of CDs can be modulated through chemical modifications.

Also, CDs have been investigated in the highly interesting field of neurodegenerative diseases associated with protein misfolding (33).

The mostly used CD in developing systems to be applied over the eyeball is 2-Hydroxypropyl-ß-cyclodextrin, since it does not show irritating effects and has improved water solubility and may be toxicologically benign (35) (36). Concerning other types of CD, the cavity size of α-CD is insufficient for many drugs, γ-CD is expensive, and, in general, δ-CD has weaker complex forming ability than conventional CDs. β-CD has been widely used in the early stages of pharmaceutical applications because of its ready availability and cavity size, which is suitable for the widest range of drugs. Nevertheless, low aqueous solubility and nephrotoxicity limited its use especially in parenteral DD (see figure 7 for a schematic representation of each cyclodextrin) (34).

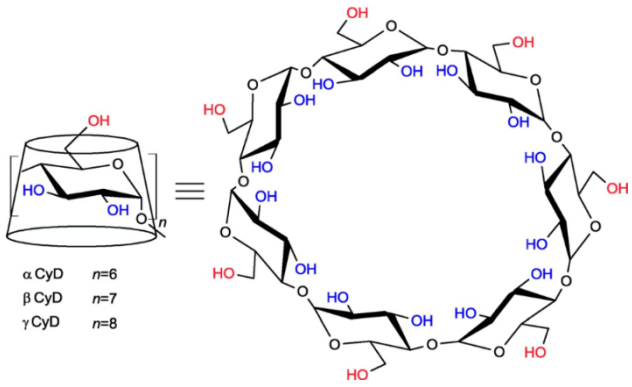

Figure 7 - Representation of the cyclodextrin macromolecule (33).

CDs have several applications in the eye-care field, especially in the aqueous eye drop preparations, to reduce ocular drug irritations and to promote the drug permeability by making the drug available in the ocular surface and increasing absorption. CDs have shown to be non-toxic to the eye and to be well-tolerated in the aqueous/biological medium (34).

The most widely used approach to study inclusion complexation is the phase solubility method, which examines the effect of a solubilizer, CD or ligand, on the drug being solubilized, the substrate. The equilibrium binding of drug and CD to form a 1:1 complex can be represented as:

$$\text{Drug} + \text{CD} \rightleftharpoons \text{Drug:CD Complex}$$

The type of CD can influence the complex formation (the cavity size of CD should be suitable to accommodate a drug molecule of a particular size) as well as the

performance of drug/CD complexes. Compared with neutral CDs, complexation can be better when the CD and the drug carry opposite charges (conversely, complexation may decrease when they carry the same charge) (34).

Figure 8 depicts the dynamic equilibrium for 1:1 (figure 8a) and 1:2 drug–CD (figure 8b) complexes. As seen, inclusion complexes may be formed involving the entire drug molecule or only a portion of it. Figure 8c presents schemes of how α-, β- and γ-CD can form inclusion complexes with a specific drug.

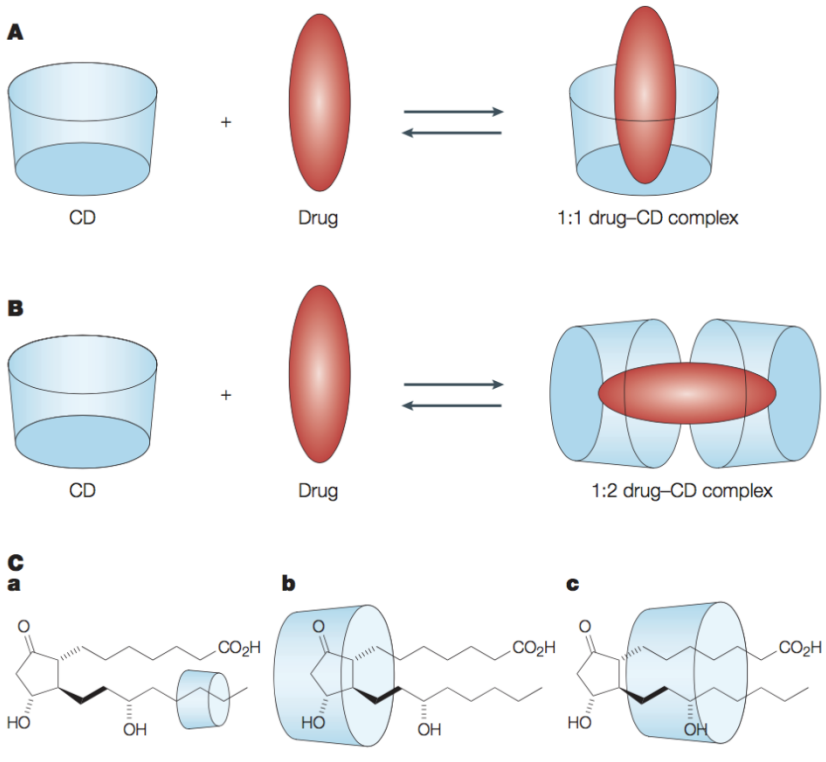

Figure 8 - Schematic illustration of the association of free cyclodextrin and drug to form drug-CD complexes. **A:** 1:1 drug-CD complex; **B**: 1:2 drug-CD complex; **C: a)** α-CD; **b)** ß-CD; **c)** δ-CD. Adapted from (1).

1.2 Motivation

The principal motivation for this research deals with the development of DD LbL films for glaucoma treatment able to release precise amounts of drug and at precise periods of time. The conventional method consists on eye drops administration, for which only 20% of the active drug in one droplet achieves the ocular anterior chamber, the remaining being drained through the nasolacrimal duct (13). Another problem relates to

the patient non-compliance, since half of glaucoma patients do not use their ophthalmic medication properly (37).

A potential alternative solution in glaucoma treatment could be the use of intralocular devices. This thesis developed DD films that can be work as coatings of an intraocular device, incorporating the same drug as that used in the conventional therapeutics.

1.3 Objectives and research overview

The objective of this research was to develop biocompatible multilayer films with DD function that can coat intraocular devices in order to be used in glaucoma treatment. The main goal was to fabricate films composed of layers of brimonidine, GO and PBAE.

The first strategy consisted in preparing GO functionalized with ß-cyclodextrin to control the number of cyclodextrins contained in the film. However, the syntheses were not well succeeded and a second approach was adopted consisting in the preparation of layers of brimonidine encapsulated in 2-Hydroxypropyl-ß-cyclodextrin. The complex was then deposited over a bilayer of charged GO by self-assembly. Thus, the DD films were composed by alternated layers of brimonidine encapsulated with 2-Hydroxypropyl-ß-cyclodextrin and two types of layers, PBAE and charged GO to control the rate of released brimonidine. The films growth was followed by atomic force microscopy (AFM) and UV-Vis absorption spectroscopy. Three types of films, where layers of brimonidine were intercalated with different sequences of layers (PBAE/GO^+/GO^-), (PBAE/GO^-/GO^+) and (GO^-/GO^+) were prepared.

The efficiency of DD films in terms of brimonidine release was followed by UV-Vis absorption spectroscopy and by High Performance Liquid Chromatography (HPLC).

1.4 Thesis Outline

This thesis is divided in four main chapters. In the Introduction, it is presented the current state of the art, regarding the inherent complications of glaucoma and its treatments. The biomedical developments that have taken place in order to treat this disease and its complications are also described. Chapter 2 describes the materials used to prepare de drug delivery films, the methods and characterization techniques used to characterize the films and the kinetic of brimonidine released. Chapter 3 presents the

results of the drug delivery films growth and its characterization by Ultraviolet-visible spectroscopy (UV-Vis) and by Atomic Force Microscopy (AFM). Chapter 4 comprises the kinetics of brimonidine release and its characterization by UV-Vis, and HPLC. Chapter 5 describes the main conclusions of this work and Chapter 6 describes proposals of future works in order to keep going this thesis. An Appendix section is presented at the end with additional results.

Chapter 2 - Materials and Methods

2. Materials and Methods

2.1 Materials

2.1.1 Negatively charged graphene oxide

Negatively charged GO was purchased from Graphenea, as an aqueous dispersion of nanosheets with a concentration of 0.5 mg/mL and 4mg/mL (see figure 9).

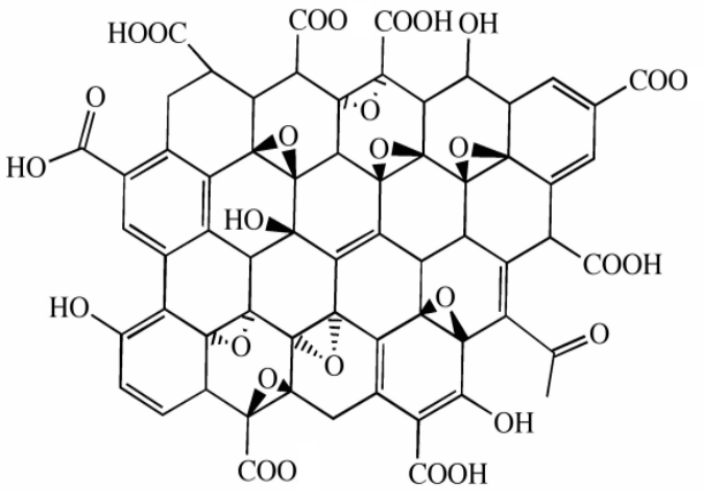

Figure 9 - Chemical structure of negatively charged graphene oxide.

2.1.2 Graphene Oxide functionalized with cyclodextrin

The first approach was to synthetize GO functionalized with the ß-cyclodextrin, following a method developed by Wang *et al.* (23). This process includes two steps, the first step was the preparation of graphene with epoxi groups to anchor CD (GO-O) and the second one, the preparation of GO-β-CD. This study also refers to a preparation of the GO by the Hummers method (38), but in this thesis, it was used the commercial GO. The negatively charged nanosheets were purchased as an aqueous dispersion with a concentration of 4 mg/mL. The method described by Wang *et al.* (23) is as follows: 10 mL of graphene oxide aqueous dispersion with a concentration of 4.0 mg/mL (pH=2.40) were mixed with 15 mL of distilled water and the mixture is homogenized in an ultrasonic bath for 10 min The pH is then adjusted to 9.44 with drops of an aqueous solution of NaOH 10%.

Next, 1.5 mL of epichlorohydrin (ECH) from Sigma Aldrich was added dropwise and this solution was stirred at room temperature for 30 min. At pH of 9.44 most hydroxyl groups in GO suffer deprotonation and a nucleophilic attack can occur to the C-Cl group in epichlorohydrin, the anchoring group. This reaction must be performed under alkaline conditions through a reaction between ECH and the –OH on the graphene. Then the temperature was gradually increased to 60ºC and the mixture was stirred magnetically at 60ºC for 3h. It is important to maintain the initial stage of the reaction at the room temperature to assure that only a nucleophilic reaction occurs, instead of an elimination reaction, which is favored by high temperatures.

The final volume obtained of the GO-O solution was 28 mL. Next, a dialysis was performed using a cellulose membrane (Sigma Aldrich), that has a cut off of about 12 000-14 000 Da. Before the dialysis, the membrane was washed for one day under running water, to remove the protective glycerol layer.

The dialysis was performed during several days in a large volume of water which was replaced every day. After the dialysis, 30 mL of a freshly prepared carbonate buffer solution with pH=10.00 prepared from two solutions of 2 mL of 0.2M $NaHCO_3$ (1.68g/100mL) and 23 mL of 0.2M K_2CO_3 (2.76g/100mL) was added. The final pH was 9.97 (V_{Final}=60mL). 0.500 g of ß- Cyclodextrin was added to the solution and the mixture was stirred magnetically at 60ºC for 3 hours. Figure 10 represents a scheme of the preparation of the GO functionalized with CD.

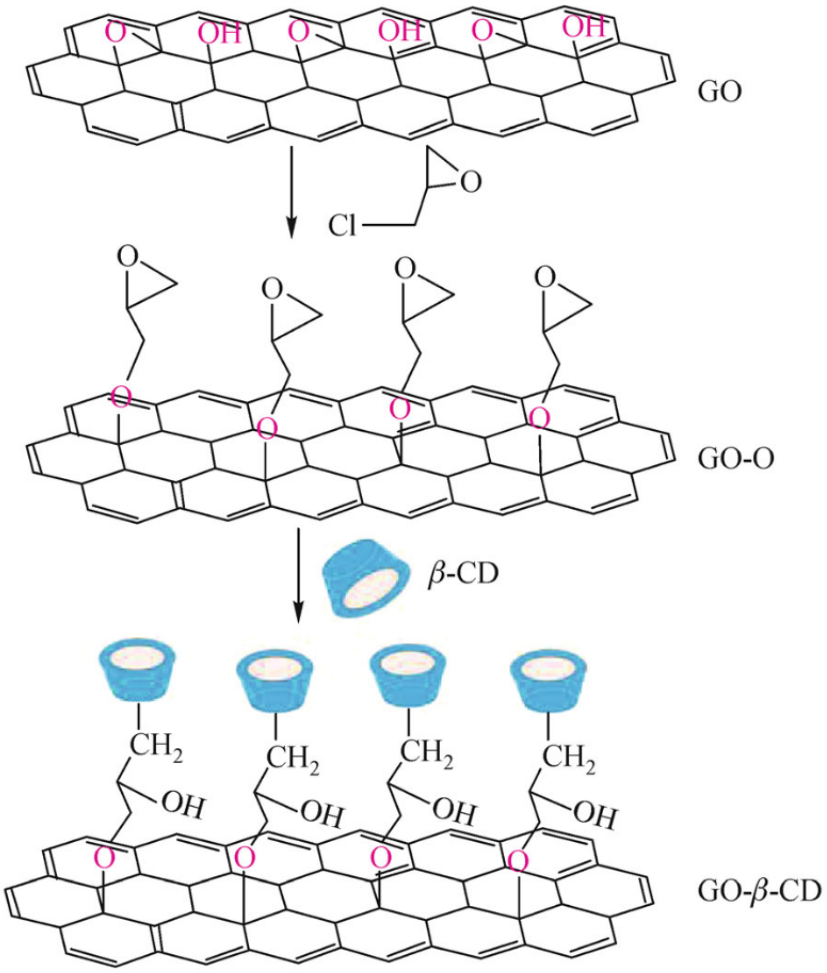

Figure 10 - Schematic illustration of the preparation of ß-CD functionalized with graphene oxide. Adapted from (23).

Unfortunately, the results obtained did not comply with those reported in literature, since by comparing the infrared spectrum of the G-ß-CD after the above described treatment and the infrared of pristine GO-O, no significant changes were observed. Figure 11 to figure 13 describes the results obtained compared with the literature (23).

It was also performed NMR to the washing waters of the dialyses performed on each step of the reaction to assure that GO-O was not left behind during that purification step. It is very likely that the used GO-O had a low density of –OH groups and therefore, for that reason, the degree of functionalization obtained is also low. To circumvent this, will be proposed that in future work, GO-O should be synthetized by Hummers method (38), as reported, instead of using commercial GO.

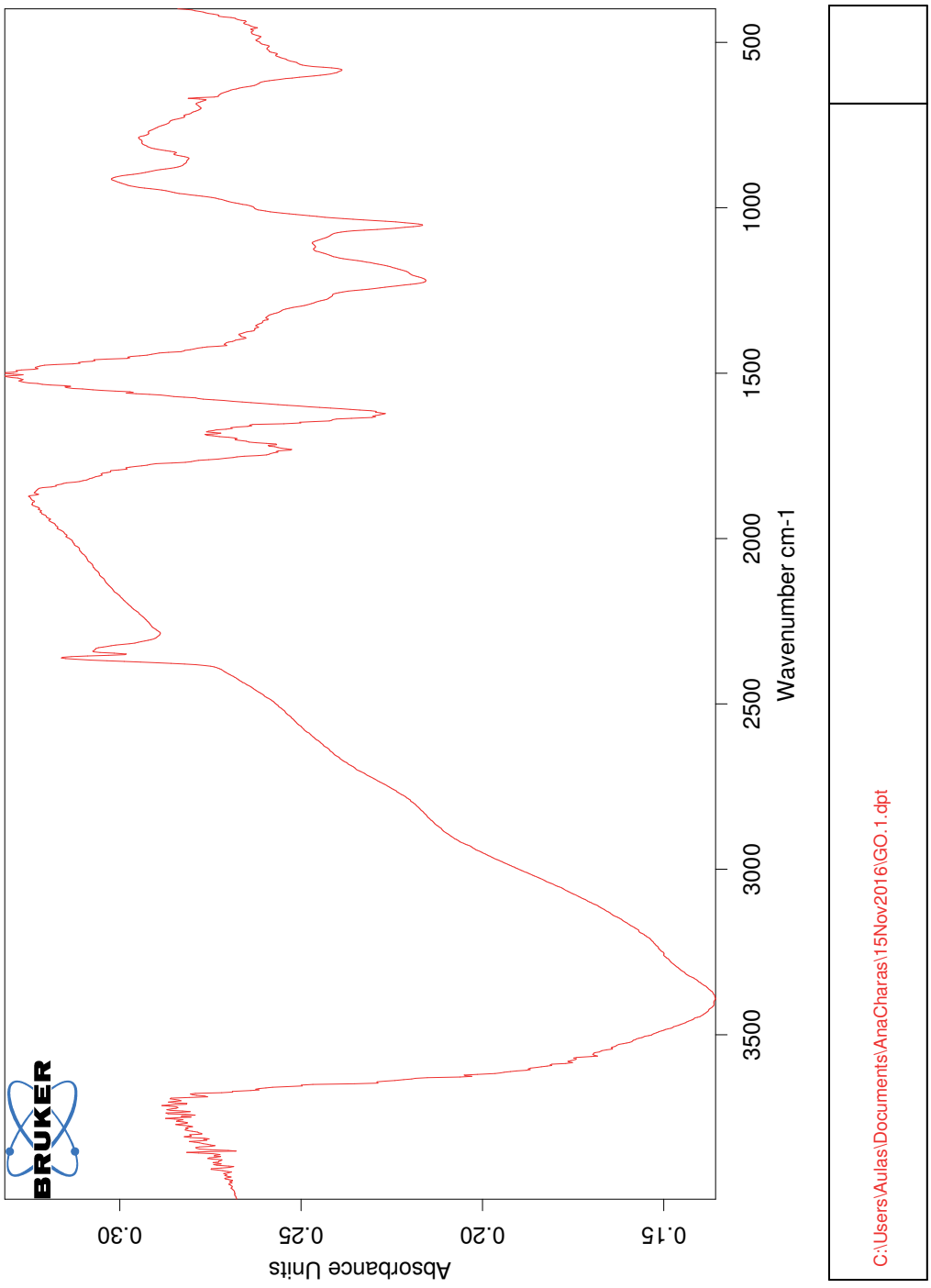

Figure 11 - Infrared spectrum of dried GO obtained in step GO deposited over a KBr pellet.

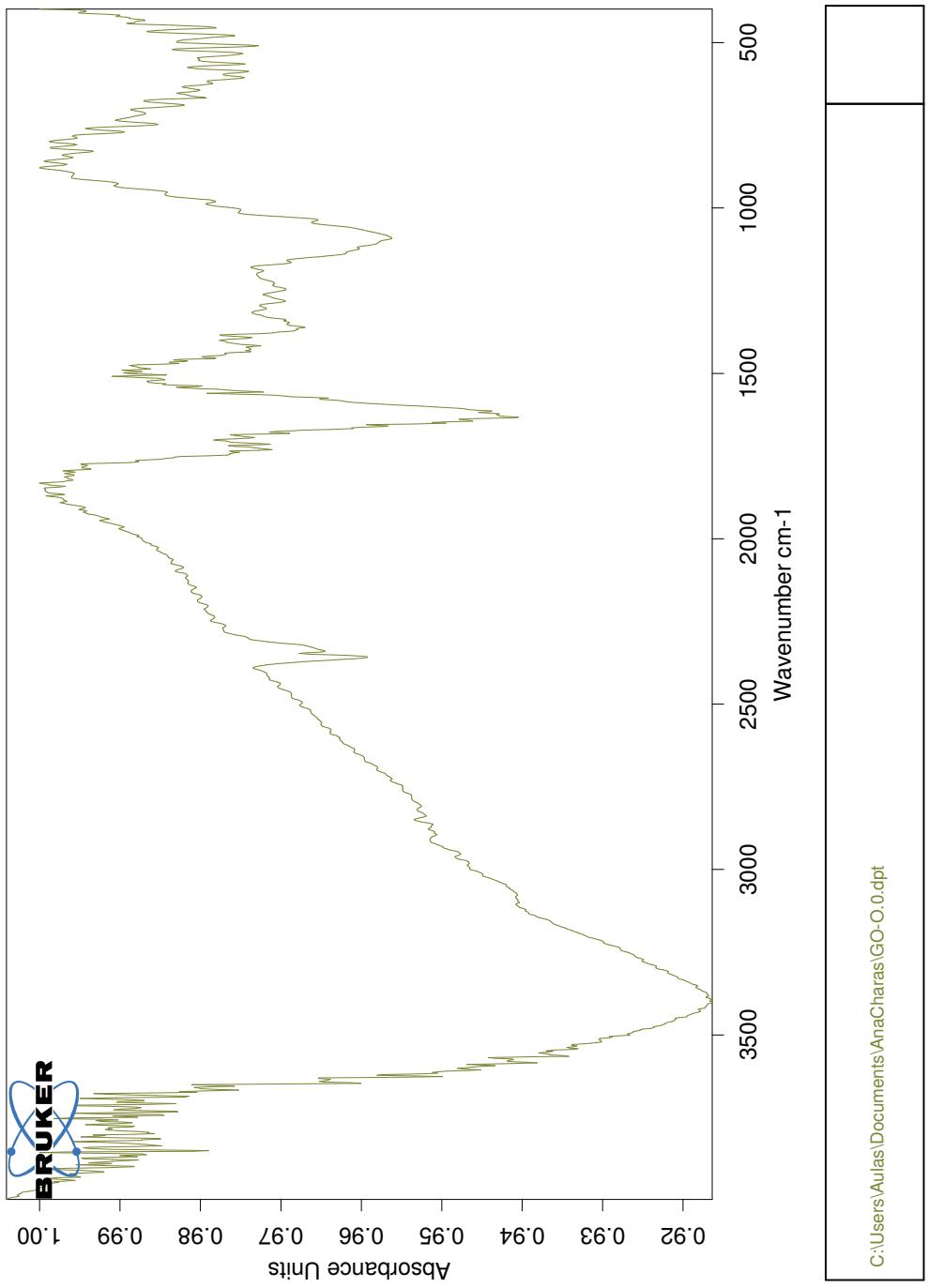

Figure 12 - Infrared spectrum of dried GO-O obtained in step GO-O deposited over a KBr pellet.

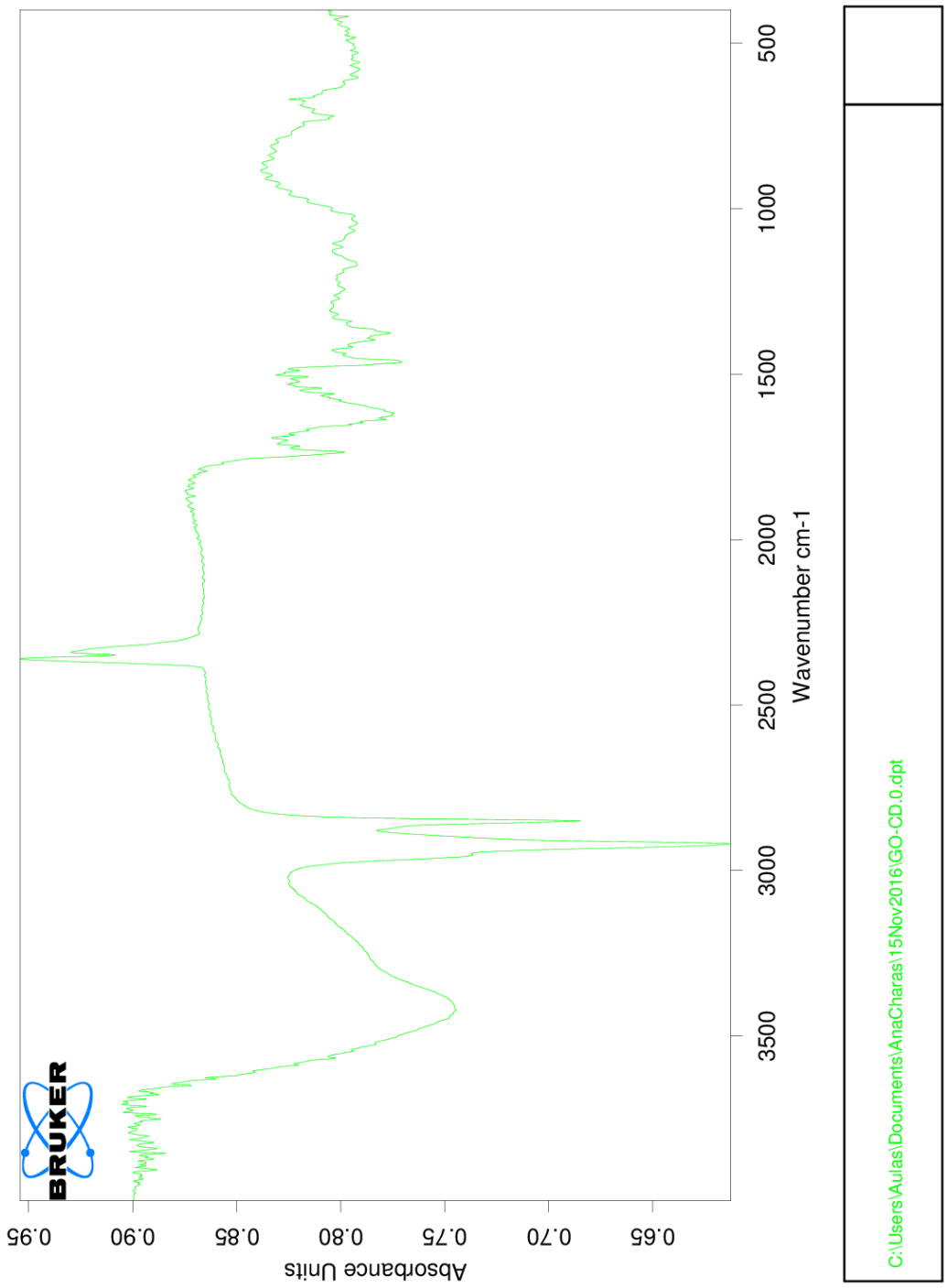

Figure 13 - Infrared spectrum of dried GO-ß-CD obtained in step GO-β-CD deposited over a KBr pellet.

2.1.3 Synthesis of positively charged graphene oxide

The positive nanosheets of GO were prepared by reducing the negative GO (in aqueous dispersion with a concentration of 0.5 mg/mL) and linking amine groups to the carboxylic acids present at the edges of the GO (see figure 14). A method developed by Hwang *et al.* (39) was used to prepare positively charged GO.

Under this method, 50 mL of negative GO solution were mixed with 0.625 g of *N*-ethyl-N'-(3-dimethylaminopropyl)carbodiimide methiodide (EDC) (Sigma Aldrich) and with 5 mL of ethylenediamine (Sigma Aldrich).

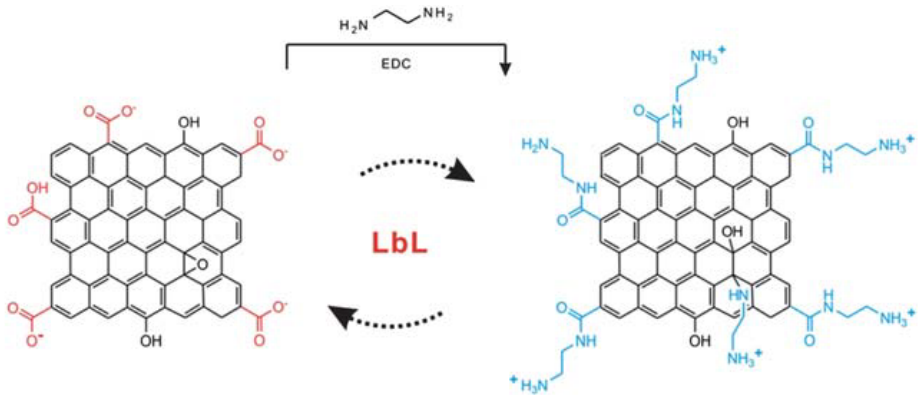

Figure 14 - Schematic representation of the reaction to obtain positively charged graphene oxide from negatively charged GO. The two GOs will be alternated by the LbL method (52).

2.1.4 Poly (ß-amino ester)

The PBAE (see figure 5 for molecular formula) used in the thesis was previously synthetized by the Organic Electronics group of IT following the protocol described by Lynn, *et al.*: 3.28 g of 4,4'-trimethylenedipiperidine (S1) (97% purity, Sigma Aldrich, CAS number 16898-52-5) and 2.87 mL of 1,4-butanediol diacrylate (S2) (99% purity, Alfa Aesar, CAS number 1070-70-8) were mixed in dry tetrahydrofuran (THF) (previously distilled). The copolymerization was carried out at a temperature of 50°C, during 48 hours. The polymer PBAE was purified through repeated precipitations into diethyl ether. The final polymer was then dried under vacuum overnight. The structure of the final product was confirmed by Nuclear Magnetic Resonance Spectroscopy (NMR) (27).

2.1.5 2-Hydroxypropyl-β-cyclodextrin

2-Hydroxypropyl-β-cyclodextrin (HP-β-CD) (figure 15), the host used to encapsulate the brimonidine, was purchased from Sigma-Aldrich (CAS number: 128446-35-5, M_w=1460 g.mol^{-1}.) and it was used as received.

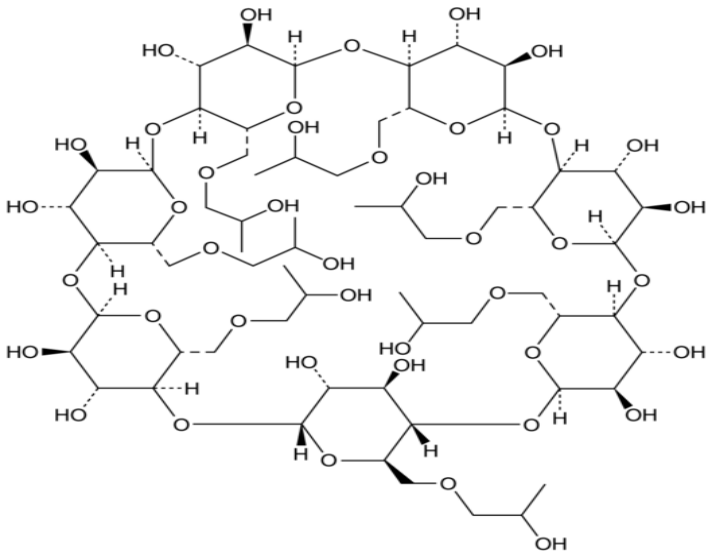

Figure 15 - Chemical representation of the 2-hydroxypropyl-β-cyclodextrin molecule.

2.1.6 Brimonidine

Brimonidine is an ocular drug usually used in glaucoma treatment, used to decrease the intraocular pressure. Brimonidine was supplied from Sigma Aldrich (Mw=292.13 g.mol 1, CAS number 59803-98-4).

2.1.6.1 Brimonidine encapsulation

Complexes of brimonidine encapsulated in (HP-β-CD) were prepared by dissolving 2.25 g of HP-ß-CD (maximum solubility is 45% (w/v)) in 3 mL of distilled H_2O, the solution was left to stir for 2 hours. Then 4 mg of brimonidine (maximum solubility: 0.8 mg/mL) was added and the volume was completed to 5 mL with distilled H_2O. This solution was stirred for 12 hours protected from light. As figure 16 shows, the absorption spectrum of the brimonidine solution shows an absorption band at 250 nm which is characteristic band of the complex HP-ß-CD (HP-ß-CD+Brim).

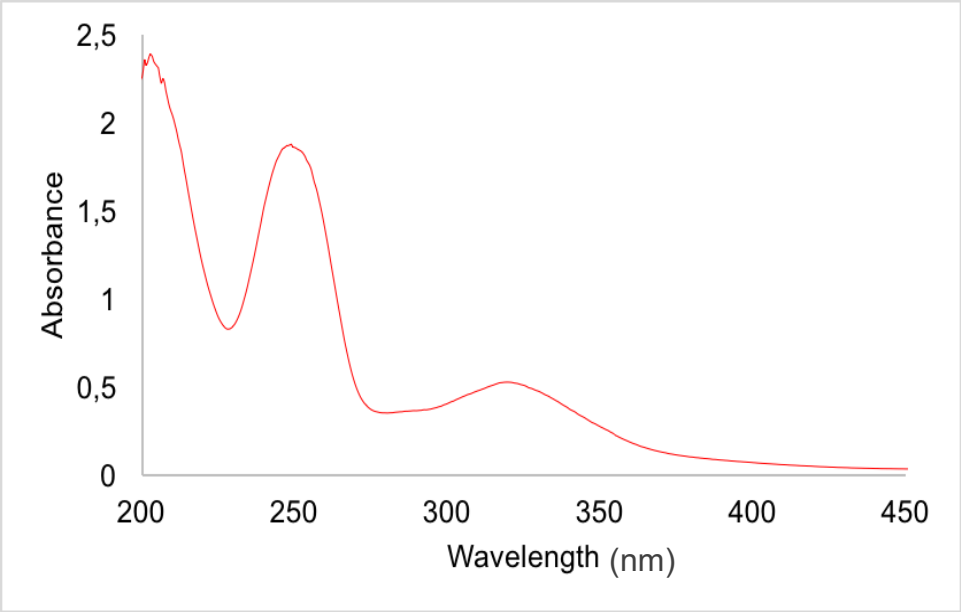

Figure 16 - UV-Vis absorption spectrum of brimonidine encapsulated in HP-ß-CD. (Concentration = 2.74 mM).

Figure 17 shows an UV-Vis absorption spectra comparing a solution of brimonidine in PBS and the solution of brimonidine after film immersion in PBS solution.

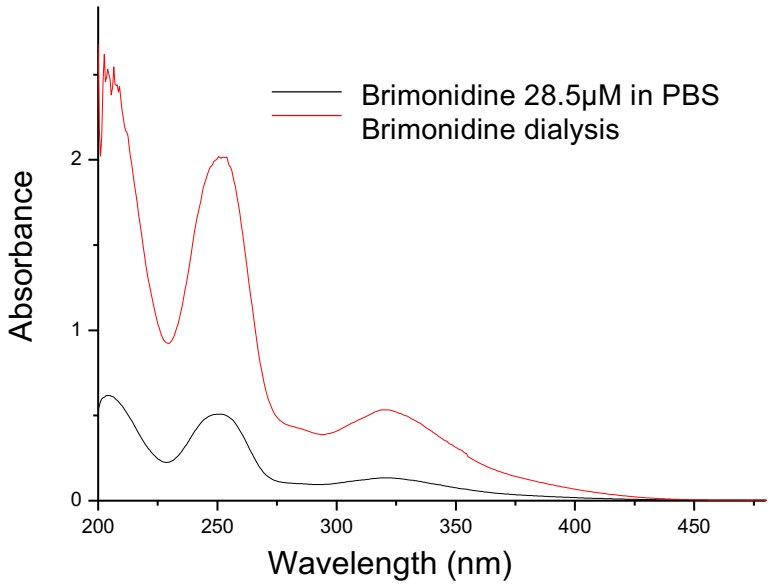

Figure 17 - UV-Vis absorption spectra of Brimonidine solutions: after dialyses and in standard PBS 28.5 µM.

2.2 Characterization techniques and DD films preparation

This section describes the techniques that were used to characterize the films and details the method employed to prepare the multilayer DD films.

2.2.1 Ultraviolet-visible absorption spectroscopy

UV-Vis spectroscopy is a technique, that comprises to absorption spectroscopy or reflectance spectroscopy in the ultraviolet-visible spectra region.

When radiation interacts with matter, several processes can occur, including reflection, scattering, absorbance, fluorescence/phosphorescence and photochemical reaction. Since light is a form of energy, absorption of light by matter causes the energy content of the molecules (or atoms) to increase (40).

The Lambert-Beer's law, is a quantitative way to determine concentrations of an absorbing species:

$$I = I_0 \cdot e^{-\mu \cdot l} \qquad \text{Equation (1)}$$

where I_0 is the initial intensity of the radioactive source, I is the remaining beam intensity, μ is the linear attenuation coefficient and l is the thickness of the absorber (41).

The maincomponents of a spectrophotometer are (40) (42), a source of radiant energy; a wavelength selector, that isolates a limited region of the spectrum; one or more sample containers; one or more detectors to measure the intensity of radiation; other optical components, such as lenses or mirrors; a computer, to process the signal. With this technique, absorption spectra of the DD films were obtained to follow the film growth after the formation of each bilayer and to quantify the brimonidine release. The absorption spectra of the films were obtained using quartz substrates. A Cecil Aquarius CE 7200 spectrophotometer was used in all experiments (see figure 41 on appendix).

2.1.2 Atomic Force Microscopy

Atomic force microscope (AFM) is one of the most important technique for morphological studies in biomedical field and it is commonly used to acquire high-resolution surface topography images (3) (43). AFM was invented in 1986 by Rohrer and Binnig (44) and has been used to image surfaces at molecular and nanoscale. Furthermore, the AFM is able to study mechanical forces and molecular interactions of

adsorbates on surfaces. The basic principle of AFM is based on a sharp tip integrated into a flexible cantilever which is brought close with the sample surface and scans the sample surface. At this stage, attractive and repulsive forces cause the deflection of the cantilever which is controlled by feedback mechanism, an optical beam apparatus detects the cantilever's deflection which is recorded and analyzed by an electronic system (45) (46).

AFM probes the surface-supported sample by scanning the tip. The tip position, which reflects the tip–surface interaction, is monitored by the deflection of a laser beam on the cantilever, which is measured by a position-sensitive quadrant photodiode. The computer and electronic system then record the cantilever position (Z) at each point of the scanned surface (X, Y) (figure 18 demonstrates the apparatus of the AFM) (45).

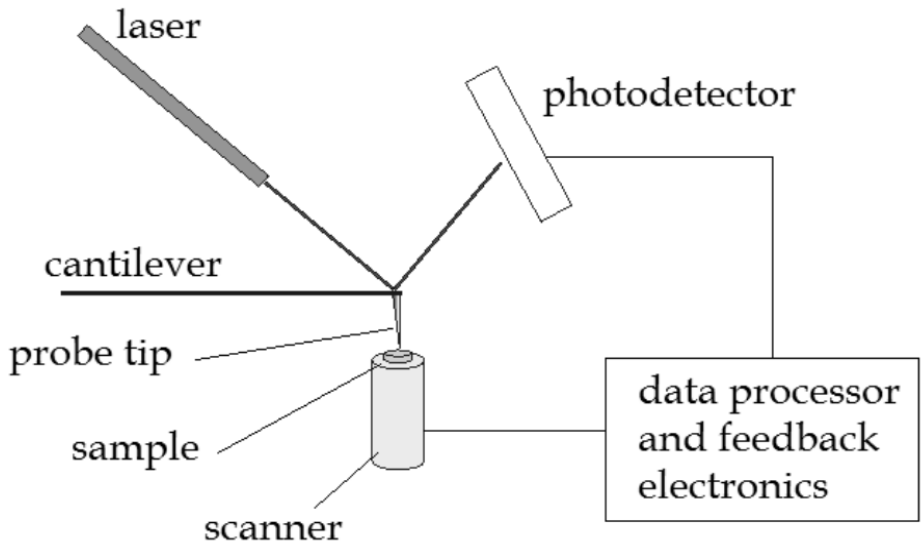

Figure 18 - Schematic representation of the AFM apparatus (2).

The AFM can operate in three types of modes, contact (the tip is in continuous contact with the surface and it's very sensitive to each small change on the surface), non-contact (the cantilever vibrates and variations from its resonance frequency are used to generate images) and intermittent (the cantilever moves rapidly with a large oscillation between the repulsive and attractive forces) (see figure 19) (3) (45) (2).

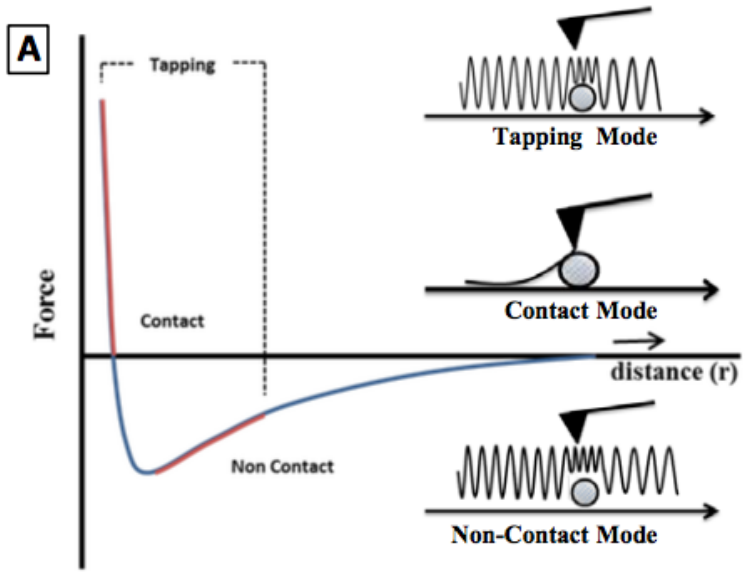

Figure 19 - Tip-sample separation curve illustrating the main interactions during AFM scanning (3).

In this work, all the measurements were performed in non-contact mode, in order to avoid damaging the studied surfaces. AFM phase contrast microscopy was used to detect and quantify changes in composition for each layer of the film (43). The topographic images were used to analyze the surface of each monolayer after adsorption. The microscope used for all the experiments was a Nano-Observer AFM from CSInstruments existing in the Organic Electronics group at Instituto de Telecomunicações (see figure 42 in appendix).

After analyzing the AFM images, it is necessary to optimize the image quality by exploring the software facilities and applying an adequate image treatment. The first step, called “levelling” is used to remove artefacts which are due to some tilt introduced in the sample image, by subtracting a background. This method is called line by line and consists in fitting an image profile line with a polynomial equation which is subtracted from that image line (47).

The surface morphology can be the described by several statistical parameters, being the amplitude parameters the principal ones for characterizing the surface topography. The Root Mean Square Roughness (Rrms) is the most used amplitude parameter; it represents the standard deviation of surface heights, and it is expressed by equation 2 (47).

The analyzed surfaces were also characterized using statistical information about the grains presented at the surface, through the calculation of the height distributions of the grains, considering that the image is constituted by a matrix with *z(x,y)* of height, with *N* lines and *M* columns.

$$Rrms\ (N,M) = \sum_{x=1}^{N} \sum_{y=1}^{M} [z(x,y) - z_{med}(N,M)]^2 \quad \text{Equation (2)}$$

2.1.3 Nuclear Magnetic Resonance

NMR is based on the interaction of magnetic moments of nuclei of various atoms with magnetic fields, this phenomenon was first described in 1946 by Bloch and Purcell. The magnetic moment of nuclei is associated with a nuclear spin, which is a form of angular momentum possessed by these nuclei. The value of nuclear spin is defined by a spin number, atoms with an odd mass number such as ^{1}H, ^{31}P and ^{13}C possess the quantum property of ‘‘spin’’ and behave as dipoles aligning along the axis of an applied magnetic field (48) (49).

In this work, it was performed NMR-^{1}H (300 MHz, $CDCl_3$) of the wash solution obtained in the synthesis of GO-O and GO-β-CD (the results obtained are shown in appendix on figure 45).

2.1.4 Infrared spectroscopy

Infrared (IR) spectroscopy is one of the most common and widely used spectroscopic techniques, very useful to identify functional groups and molecular structures (50) (51). Basically, it is an absorption spectroscopy which probes samples absorption of the infrared electromagnetic radiation. In this work, it was determined Fourier-transform infrared (FTIR) absorption spectra, obtained by transmission, of the GO, GO-O and GO-β-CD in each step on the synthesis, it was used a Bruker spectrometer.

2.1.5 DD Films Preparation

Firstly, all the used substrates were washed in «piranha solution», this process consists of immersing the sample in a mixture of H_2SO_4 and H_2O_2 to oxidize surface contaminants (i.e. to remove any organic contamination), then washed with copious amounts of tap water and finally they were submitted to a sequence of washes with distilled water, propan-2-ol HPLC, and again distilled water. The substrates were then dried with a nitrogen gas flow.

In order to improve the adsorption of the first layer of PBAE, it was necessary to increase the hydrophilicity of the substrate surface (52). The substrates were treated with oxygen plasma in a vacuum chamber Plasma Prep 2 from, Gala Instrument (see figure 43). The optimum time of absorption was previously studied (53), each substrate was immersed for 5 minutes onto each solution.

After the treatment with oxygen plasma, the substrate was immersed into a solution of PBAE. After remaining in this solution for a certain period of time, the substrate was rinsed with an aqueous solution of sodium acetate (with pH adjusted to 5.0) in order to remove non adsorbed molecules (only physically adsorbed) and then it was dried with a nitrogen gas flow. After this sequence, a monolayer of PBAE is formed. Then the substrate was immersed in the solution of positively charged GO, during a certain period of time and washed again in sodium acetate (pH=5.0). It was, dried with nitrogen, and the substrate was immersed again, now into a solution of negatively charged GO, during a certain period of time, and washed in sodium acetate (pH=5.0). After drying with nitrogen, finally the substrate was immersed into a solution containing brimonidine encapsulated with HP-ß-CD, during a certain period of time, washed in sodium acetate (pH=5.0) and dried with nitrogen. After each added layer, an UV-Vis measurement of the substrate was performed. For the film with the inverted bilayer of GO, the procedure was the same, only changing the order of immersion on the GO aqueous dispersions.

This process represents a complete cycle of the LbL assembly, forming one bilayer of (PBAE/GO^+/GO^-/HP-ß-CD+Brim) or (PBAE/GO^-/GO^+/HP-ß-CD+Brim). The deposition cycle was repeated the number of times equivalent to the number of intended bilayers.

2.1.6 High Performance Liquid Chromatography

HPLC represents the culmination of the modernization of Liquid Chromatography (LC) and is currently one of the most used separation techniques in analytical chemistry, due to its advantageous characteristics, such as high sensitivity and automation (54). The apparatus of a HPLC (see figure 20) consists of a system of distribution of mobile phase (reagent reservoir and pumping system), an injector which can be automatic or not, the column where the analytes are separated, a detector and a data acquisition system (55) (56).

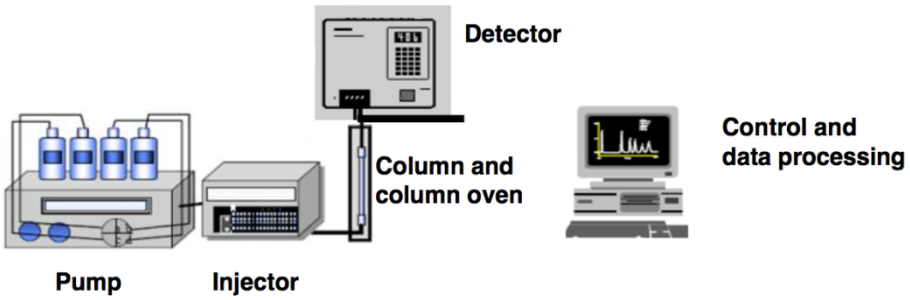

Figure 20 - High Performance Liquid Chromatography apparatus (Adapted from (4)).

In addition, most recent HPLC systems also contain a degassing system to remove gases dissolved in the solvents and which may affect the performance of the detector. The pumping system of an HPLC apparatus is capable of pumping the mobile phase at a specific flow rate and at high pressures so as to be able to traverse the column. From this system, there are also devices that allow to control the flow and to program the proportion of each of the solvents used in the mobile phase, in case of a gradient elution (56) (54). The sample, dissolved in the mobile phase, goes to the chromatographic column, where the various analytes of interest are separated based on mechanisms of interaction between the mobile phase and the stationary phase. Nowadays there is a huge variety of fillers for the HPLC column, that will determine the success of the analytical method in terms of efficiency and selectivity in separating the species of interest. The analytes, according to their affinity for the stationary phase, are eluted from the column and pass through a detector, which emits a signal to a computer software. The signal is plotted as a function of the retention time, designated by chromatogram. The identification of the analytes is done based on the retention times and, from the area of the respective peaks, it is possible to quantify them (56) (4).

The HPLC analysis were performed at Instituto Superior de Engenharia de Lisboa, that kindly supplied the equipment to carry out these experiments. It was used an Elite LaChrom system (see figure 44 in appendix) with the conditions detailed on table 1. This study was based on the article found on the literature (57).

Table 1 - Chromatographic conditions used on HPLC.

Parameters	**Conditions**
Mobile Phase composition	Ammonium acetate (pH 5.0, 0.01M) - Methanol (40:60 v/v)
Flow	1 mL/min
Injection volume	20 µL
Wavelength	254 nm
Oven Temperature	30 ºC
Run time	10 minutes

Chapter 3 - Growth of drug delivery films

3. Growth of drug delivery films

This chapter addresses the growth of DD films prepared by LbL technique and monitorized by AFM and UV-Vis spectroscopy. The AFM was used to analyze the evolution of layers' morphology in order to detect imperfections during the film growth. These results were accompanied with UV-Vis spectroscopy analysis of all film layers. The following sections describe such results.

3.1 Atomic Force Microscopy analysis of DD films

The AFM technique was applied to characterize six different surfaces, in order to verify if the film was well deposited on each layer and to detect possible defects related with contaminations or roughness irregularities. Ideally, each new layer should fully coat the previous one. However, interdifusion between consecutive layers can occur leading to features that may be detected by AFM analysis, mainly through the phase images.

Phase images are obtained during the surface scanning together with the topography images; they give information about the surface homogeneity in terms of their composition. In case of occurring interdifusion between consecutive layers, the surface will be composed of more than one compound and this will result very likely as a contrast in phase images. Films with (PBAE/GO^{+}/GO^{-}/HP-ß-CD+Brim) where analyzed and all measurements were performed in non-contact mode using silicon tips. The images have a resolution of 256x256 pixels and a scanned area of 1x1 μm^2. Additional images with 2x2 μm^2 are presented in appendix (table 5 and 6). Tables 2 and 3 show the topography and phases images of all film layers and a profile line in order to characterize the roughness of each layer. It was used the same adsorption time described in section 2.1.5.

Table 2 - AFM images of prepared LbL films with different layers.

PBAE – Scan size 1 µm		
Topography	Phase	Profile line
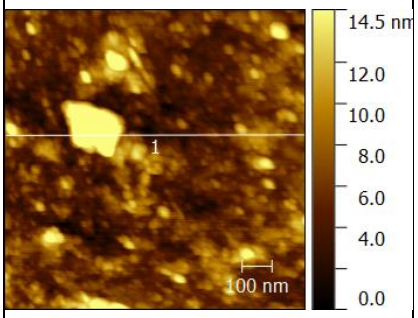	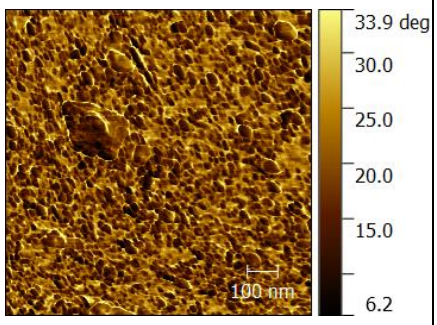	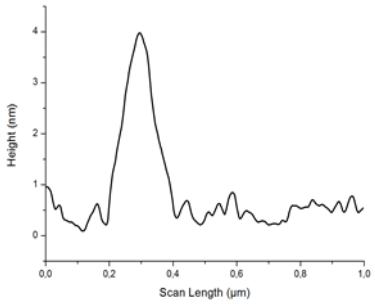
PBAE/GO^{+}/GO^{-} – Scan size 1 µm		
Topography	Phase	Profile line
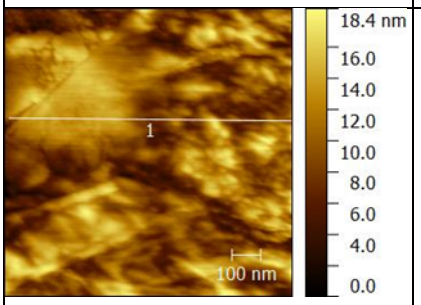	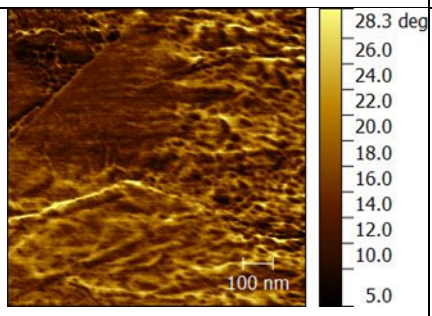	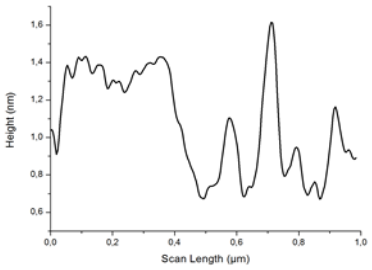
PBAE/GO^{+}/GO^{-}/HP-ß-CD+Brim – Scan size 1 µm		
Topography	Phase	Profile line
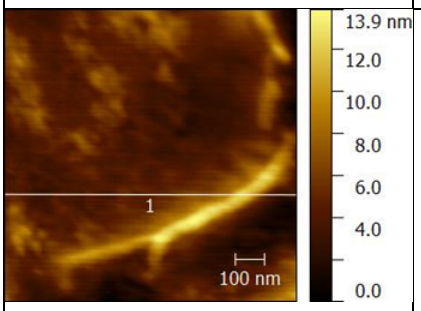	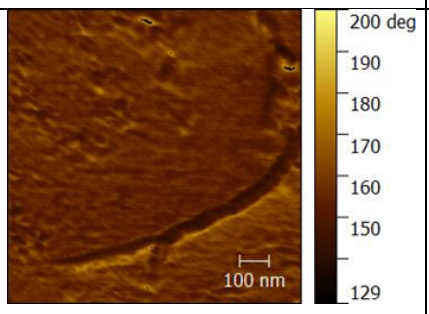	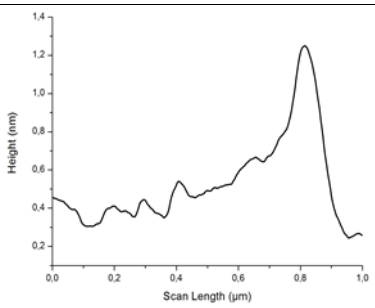

Table 3 - AFM images of prepared LbL films with different layers.

(PBAE/GO$^+$/GO$^-$/HP-ß-CD+Brim/PBAE) – Scan size 1 µm		
Topography	Phase	Profile line
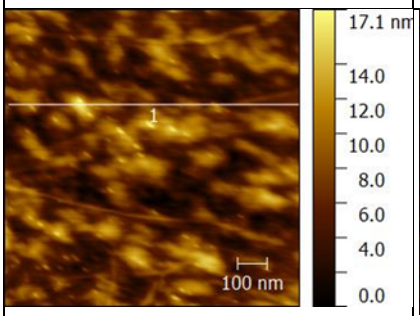	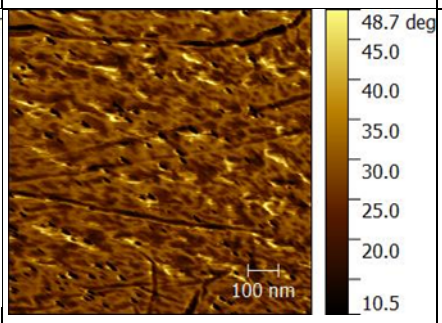	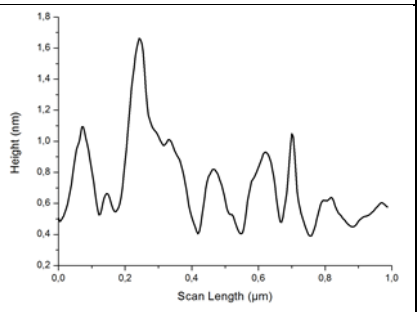
PBAE/GO$^+$/GO$^-$/HP-ß-CD+Brim/PBAE/GO$^+$/GO$^-$ – Scan size 1 µm		
Topography	Phase	Profile line
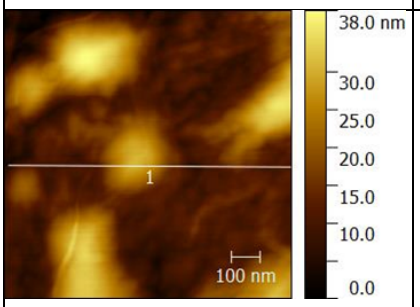	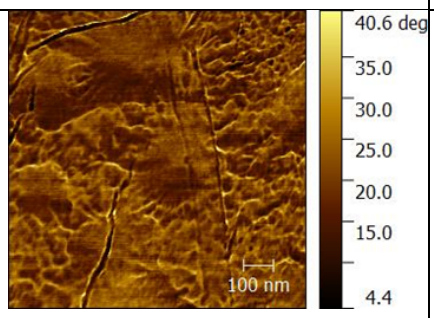	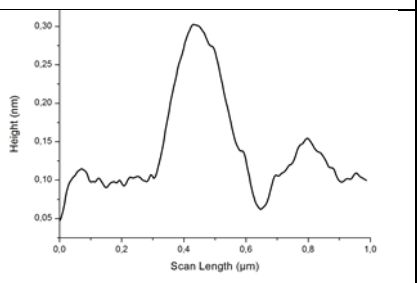
PBAE/GO$^+$/GO$^-$/HP-ß-CD+Brim/GO$^+$/GO$^-$ – Scan size 1 µm		
Topography	Phase	Profile line
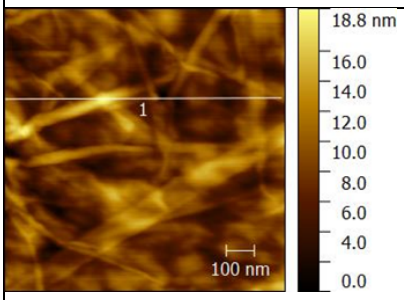	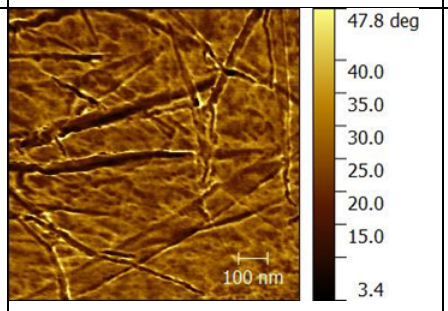	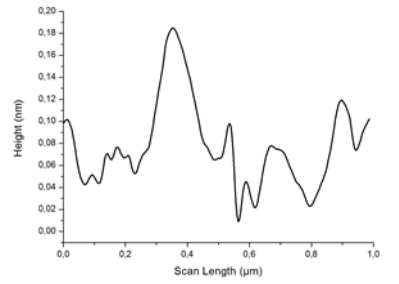

From table 2, it can be observed that the topography and phase images of PBAE surface reveal the existence of grains, also evidenced in different tip-surface interactions, i.e., when scanning the darker regions, the tip tilt is different from that in the bright ones. Such contrast in the phase image suggests the existence of two materials at the surface. Considering the fabrication approach of the films, the observed darker regions may correspond to salt grains resulting from the wash solution used after layer formation.

The AFM images of (PBAE/GO^+/GO^-) layer show a smoother surface compared with that of PBAE, exhibiting a Rrms of approximately 3.19 nm determined for the image with the scan size of 1 μm. The topography image presents straight lines which could correspond to GO nanosheets overlapping. The respective phase image shows a slight contrast between the grains and the background which can suggest the presence of salts resulting from the wash solution. Given the significant differences between the images of this film with those of PBAE film along all the extension of the scan, it can be inferred that the GO layer fully covers the previous PBAE layer.

The topographic and phase images of the (PBAE/GO^+/GO^-/HP-ß-CD+Brim) film, show a smooth surface with a Rrms of 1.97 nm. However, the phase image shows that the elevated line shown in the topographic image has a darker color compared with the background. This region can be related with GO within the previous layer which is not fully covered by brimonidine.

Table 3 shows AFM images of a PBAE layer adsorbed over the (PBAE/GO^+/GO^- /HP-ß-CD+Brim). As it may be observed, the surface is smoother (Rrms=2.73 nm) than that found for when PBAE is deposited on bare glass (Rrms of 3.64 nm). Also, the phase image suggests that the previous graphene layer is fully covered. The following images, for the bilayer of GO^+/GO^- show also a rougher surface (Rrms=7.47 nm) compared with the previous graphene bilayer (Rrms=3.19 nm).

Another film with (PBAE/GO^+/GO^-/HP-ß-CD+Brim/GO^+/GO^-) structure was analyzed by AFM in order to analyze the GO surface when GO is deposited over HP-ß-CD+Brim instead of PBAE as in the previous film. In the (PBAE/GO^+/GO^-/HP-ß-CD+Brim/GO^+/GO^-) film the surface shows a Rrms of 2.71 nm revealing to be smoother than the surface of (PBAE/GO^+/GO^-/HP-ß-CD+Brim/PBAE/GO^+/GO^-) (Rrms=7.47 nm).

3.2 UV-Vis spectroscopy analysis of DD films

The LbL films growth was studied by UV-Vis spectroscopy to characterize the kinetics of adsorption. Thus, the films were grown on quartz substrates which were firstly cleaned in a «piranha» solution to remove organic contaminants from the surface. The subtracts were treated with oxygen plasma in a vacuum chamber to improve hydrophilicity of the surface, as previously referred on section 2.1.5.

Since this is a strongly oxidizing solution, it will also hydroxylate the substrate surface, adding -OH groups, and making it highly hydrophilic; figure 21 shows schematically the effect of «piranha» on quartz (58) (59) (5).

Figure 21 - Effect of piranha treatment on quartz substrates (5).

Three types of films were analyzed in terms of their growth and they are schematized in figure 22 a, b and c. Films with and without PBAE where compared in order to analyze the influence of this polymer in the film growth and films with inverted charged graphene layers were also compared.

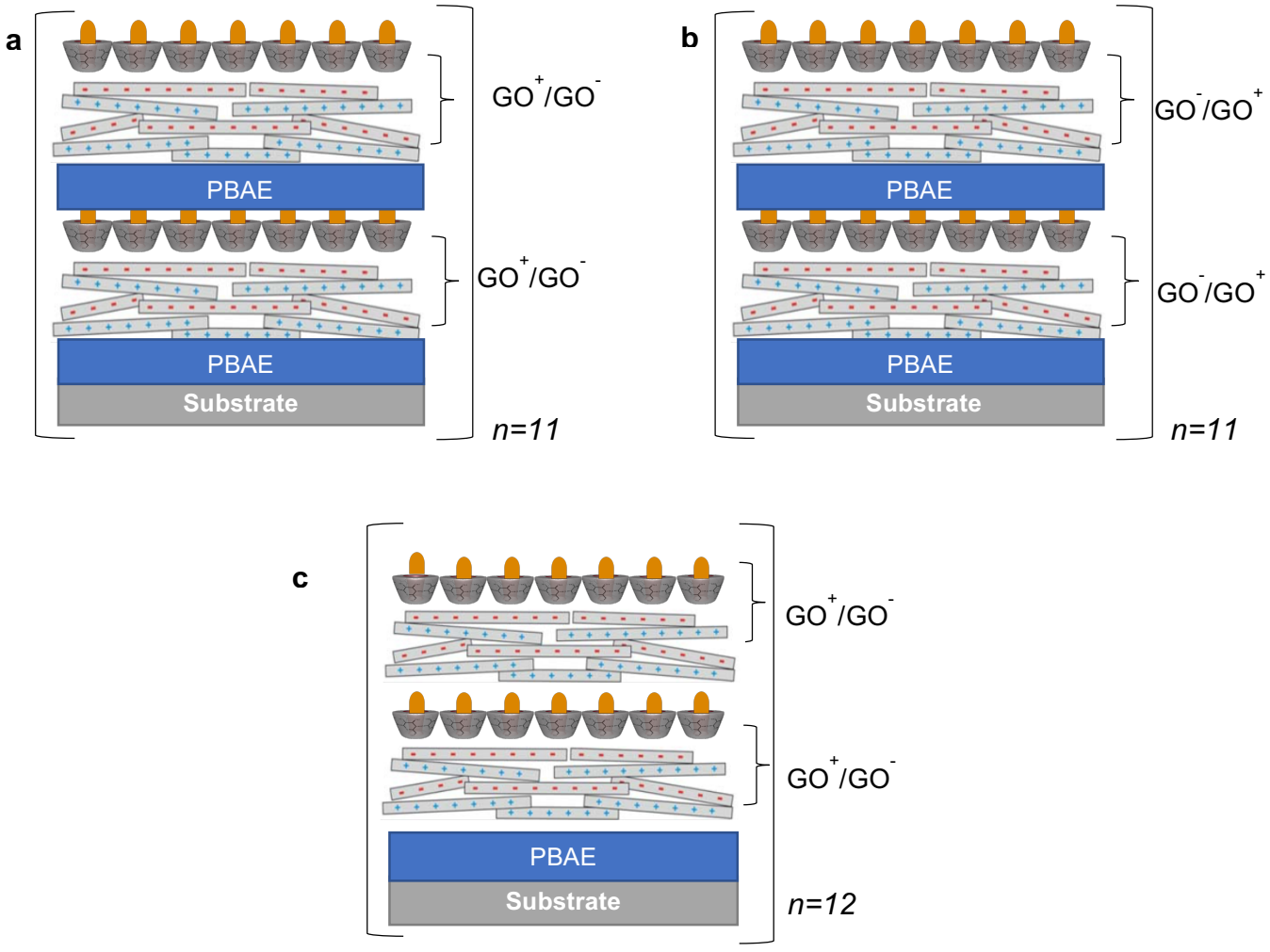

Figure 22 - Schemes of structures of a) Film with PBAE/GO^+/GO^-/HP-ß-CD+Brim; b) Film with PBAE/GO^-/GO^+/ HP-ß-CD+Brim; c) Film without intercalated PBAE. n= number of cycle layers.

3.2.1 DD films with graphene oxide films and with PBAE

Figure 23 shows the absorption spectra accompanying the growth of a film composed of eleven groups of (PBAE/GO^+/GO^-/HP-ß-CD+Brim). An UV-Vis spectrum was obtained after GO^+, GO^- and HP-ß-CD+Brim layers formation in order to monitorize the film growth step-by-step. As observed, the spectra are sequential in intensity, except for the first two layers where the spectra overlap. This behavior can be due to imperfections in the film related with incomplete layer formation.

Through the AFM analysis of the topographic and phase image of (PBAE/GO^+/GO^-/HP-ß-CD+Brim) films it was observed that the thickness of HP-ß-CD+Brim layers is not enough to cover the previous graphene bilayer. This incomplete coverage can affect the film growth. However, figure 23 indicates that absorption increases sequentially with the number of (PBAE/GO^+/GO^-/HP-ß-CD+Brim) group layers.

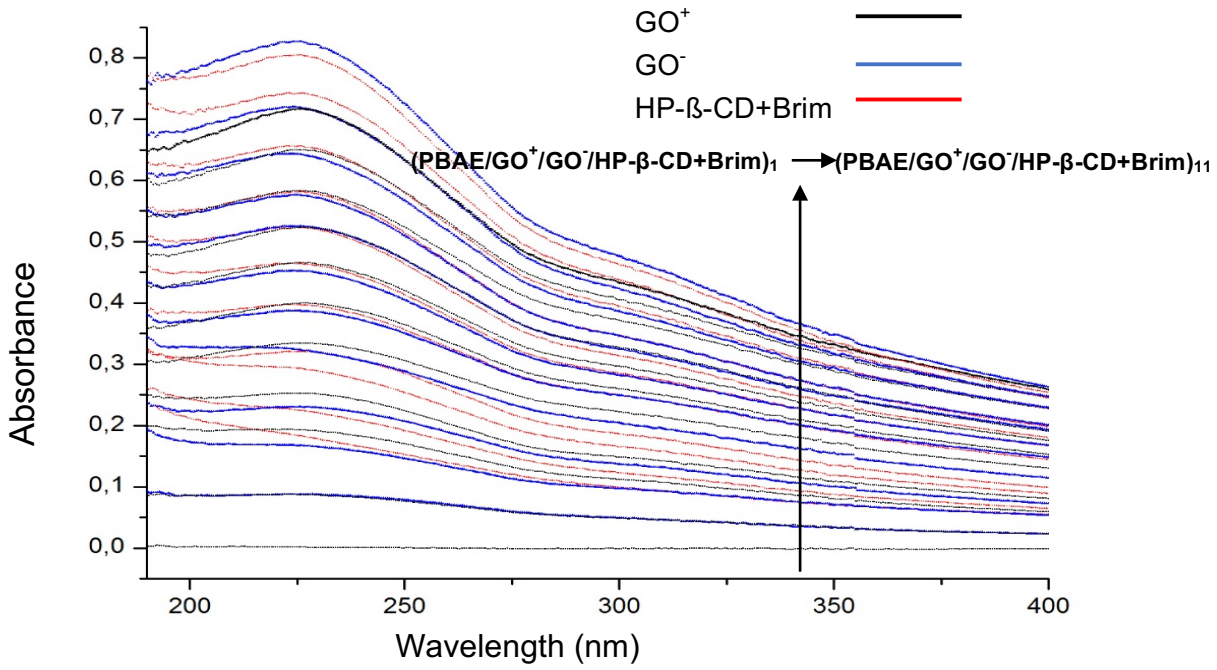

Figure 23 - Absorption spectrum of the layers presented in a film with eleven groups of (PBAE/GO^+/G /HP-ß-CD+Brim) obtained after each layer deposition.

Another type of films that were prepared and studied consisted of films where the order of GO layers was inverted, i.e. films with (PBAE/GO^-/GO^+/HP-ß-CD+Brim) groups. The objective was to observe the possible influence of the GO charge in the brimonidine absorption.

Figure 24 shows the evolution of the spectra obtained after each layer deposition for a film composed by eleven groups of (PBAE/GO^-/GO^+/HP-ß-CD+Brim).

Similarly, to the previous film, the spectra intensity also increases sequentially with the film growth. However, and similarly to what was observed for the previous film (see figure 23), some spectra sobrepositions occur for the first layers, which can also be related with incomplete coverage of the GO surface by the HP-ß-CD+Brim layer.

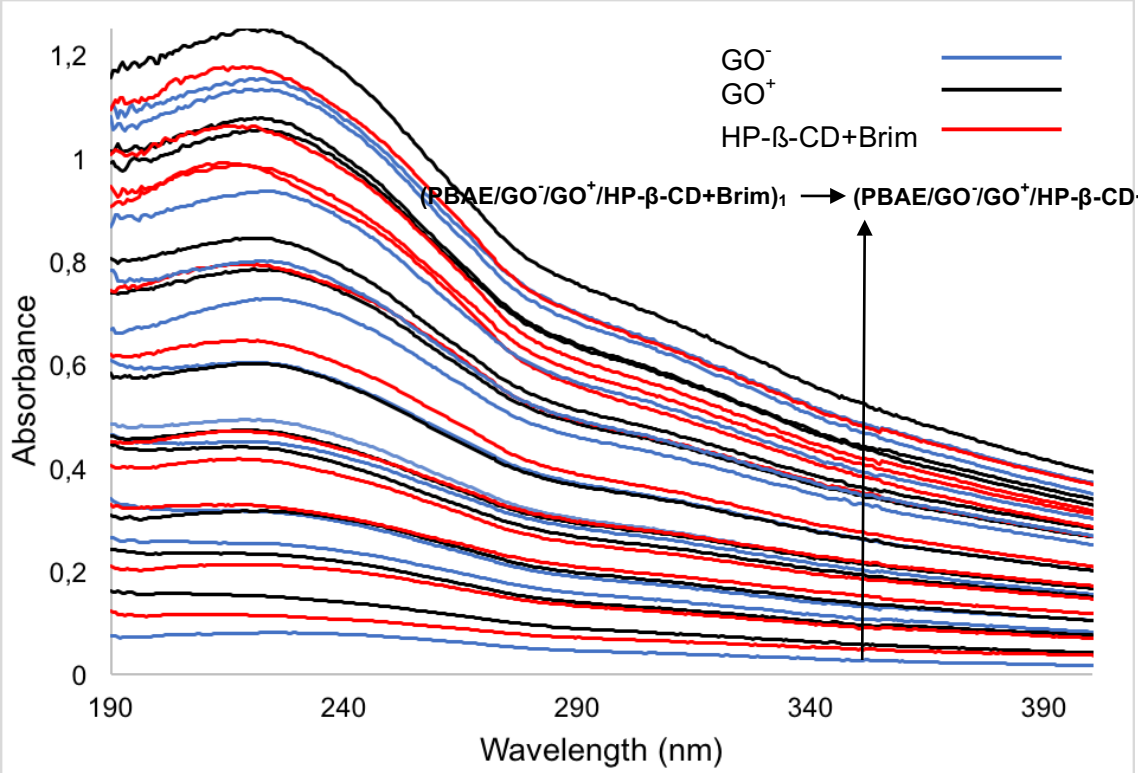

Figure 24 - Absorption spectrum of a film with eleven groups of (PBAE/GO^-/GO^+/HP-ß-CD+Brim) obtained after each layer deposition.

3.2.2 DD films with graphene oxide films and without PBAE

Figure 25 shows the absorption spectra obtained when accompanying the growth of a DD film without PBAE (film scheme in figure 21c) and with 12 groups of $(PBAE/GO^+/GO^-/HP\text{-}ß\text{-}CD+Brim/GO^+/GO^-)_{12}$. In this case, the spectra indicate that the

growth of layers is not sequential in intensity. In conclusion, the absence of PBAE can allow the interdifusion of consecutive layers, thereby causing a disorder in the film growth.

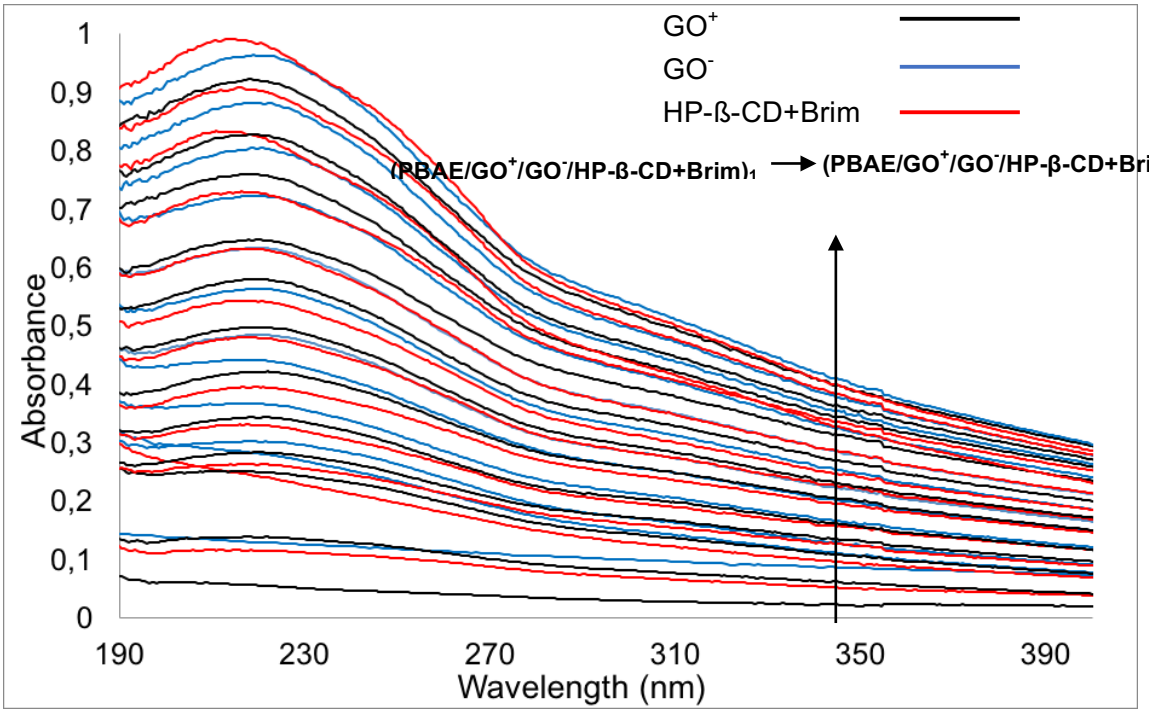

Figure 25 - Absorption spectra of the film with twelve groups (PBAE/GO^+/GO^-/HP-ß-CD+Brim/GO^+/GO^-)$_{12}$ obtained after each layer deposition.

3.3 Growth of DD films conclusion

To conclude this chapter, it is possible to draw a conclusion that the film growth in the DD films studied (see figure 22 a) and b)) is constant, and the absorption increases sequentially with the number of (PBAE/GO^+/GO^-/HP-ß-CD+Brim) group layers, and with the inverted order of GO layers the behavior is identical. Some sobrepositions occurred for the first layers and that could be related with incomplete coverage of the GO surface by the HP-ß-CD+Brim layer. For the film (PBAE/GO^+/GO^-/HP-ß-CD+Brim/GO^+/GO^-), the absence of PBAE can allow interdifusion of consecutive layers, thereby causing a disorder in the film growth.

Chapter 4 – Drug Delivery Films Release Kinetics

4. Drug Delivery Films Release Kinetics

This chapter describes the brimonidine kinetic release for the films with PBAE and graphene where three groups of films were studied: films with GO^+/GO^-, films with inverted graphene charges GO^-/GO^+ and films without PBAE. The release of brimonidine was followed by UV-Vis absorption Spectroscopy and by HPLC.

4.1 Brimonidine release kinetics of films with GO^+/GO^-

The brimonidine release kinetic was analyzed by using the techniques UV-Vis absorption and HPLC. For such analysis, the films were immersed in a phosphate buffer saline (PBS) solution which is similar to the biological fluid, in terms of pH (pH=7.4, equal to the physiologic pH) and concentration of salts, the temperature of the solution was at room temperature. A film with eleven groups of (PBAE/GO^+/GO^-/HP-ß-CD+Brim) was immersed in PBS solution during a total time of 700 hours (approximately 30 days). The immersion was controlled step-by-step, immersing the film during small periods and changing the PBS after each immersion.

After each film immersion, the PBS solution was analyzed by HPLC in order to evaluate the amount of HP-ß-CD+Brim released to the aqueous environment. To determine the brimonidine concentration in each sample, it was necessary to perform a calibration curve with standards of different concentrations.

The graph in figure 26 shows the obtained calibration curve (peak area obtained from the chromatograms *vs*. concentration) using five standard solutions with brimonidine concentrations of 4 µg/mL, 10 µg/mL, 15 µg/mL, 20 µg/mL e 24 µg/mL (see appendix figures 49 to 53 for the obtained chromatograms).

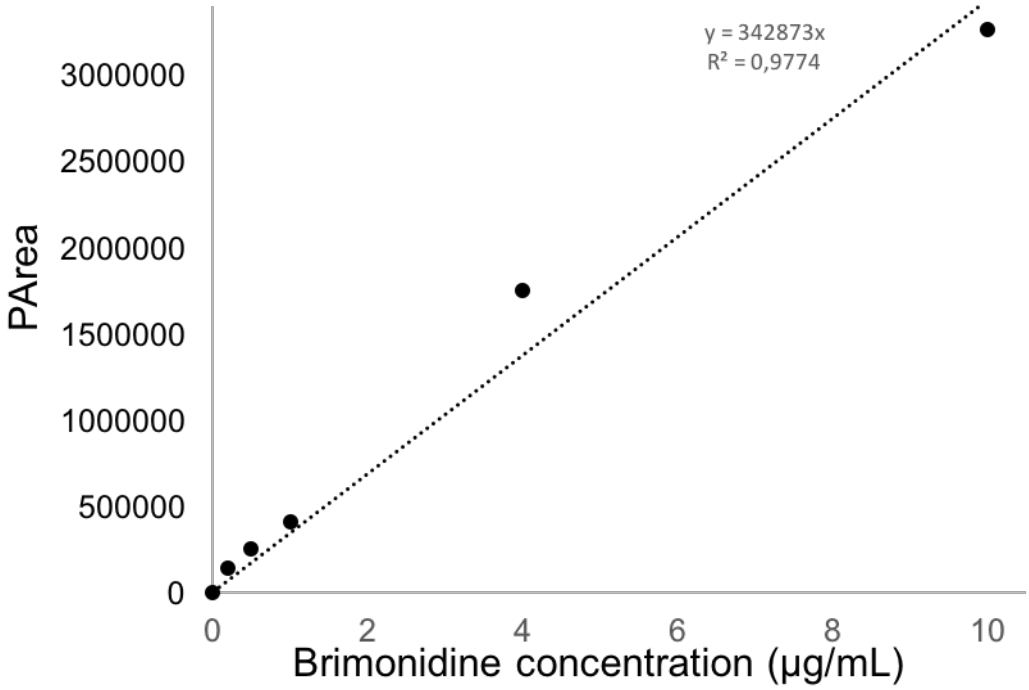

Figure 26 - Linear Regression obtained from the HPLC data.

The calibration curve was adjusted with a linear function and expressed by the equation (3). This equation allows the calculation of the brimonidine concentration in the samples from the peak area of the brimonidine in the respective chromatogram.

$$P_{area} = 342873 \times \mathrm{Brim} \qquad \text{Equation (3)}$$

For example, for the chromatogram represented in figure 27, which has an area of brimonidine of 211298 (retention time of brimonidine at 2.113 min, see table 4), will have a concentration of 0.616 µg/mL as it is demonstrated by equation (4):

$$P_{area} = 342873 \times \mathrm{Brim} + \Leftrightarrow Brim = \frac{211298}{342873} = 0.616 \frac{\mu g}{mL} \qquad \text{Equation (4)}$$

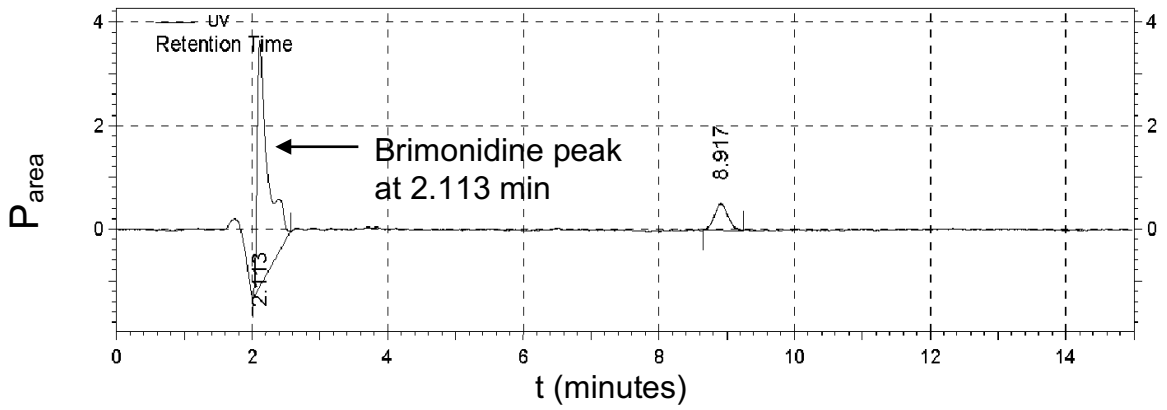

Figure 27 - Chromatogram obtained from the analysis of PBS solution after film immersion.

The area of each peak is calculated by the HPLC software *EZ Chrom Lite* which allows the identification of the peaks and automatically calculates the retention time, area, % area and the height of each peak present at the chromatogram, as described in the table 4.

Table 4 - Data obtained from the analysis of a chromatogram.

Retention Time	Area	% area	Height
2.113	211298	88.00	90.26
9,917	28824	12.00	9.74

The obtained chromatograms only show the presence of brimonidine, thus suggesting that the drug is released from the CD when the film is immersed in the PBS solution. The graph in figure 28 shows the evolution of brimonidine concentration as a function of time over a total of 30 days (all the HPLC results obtained can be consulted on figure 46 on Appendix).

After 3 hours from the beginning of the desorption study, it is possible to observe that the amount of HP-ß-CD+Brim released is approximately 0.63 µg/mL).

At approximately 50 hours the release of HP-ß-CD+Brim decreases and stays relatively stable until approximately 160 hours of immersion time, when an increase of HP-ß-CD+Brim released is observed. This release decreases a little again and stays stable until approximately 600 hours when it is possible to observe another increase of HP-ß-CD+Brim concentration (about 0.74 µg/mL).

After almost 700 hours (about 28 days) of immersion time, the amount of brimonidine released is very low comparing to the other results, this may be due to the fact that the film at this stage is composed of only the first layer of HP-ß-CD+Brim.

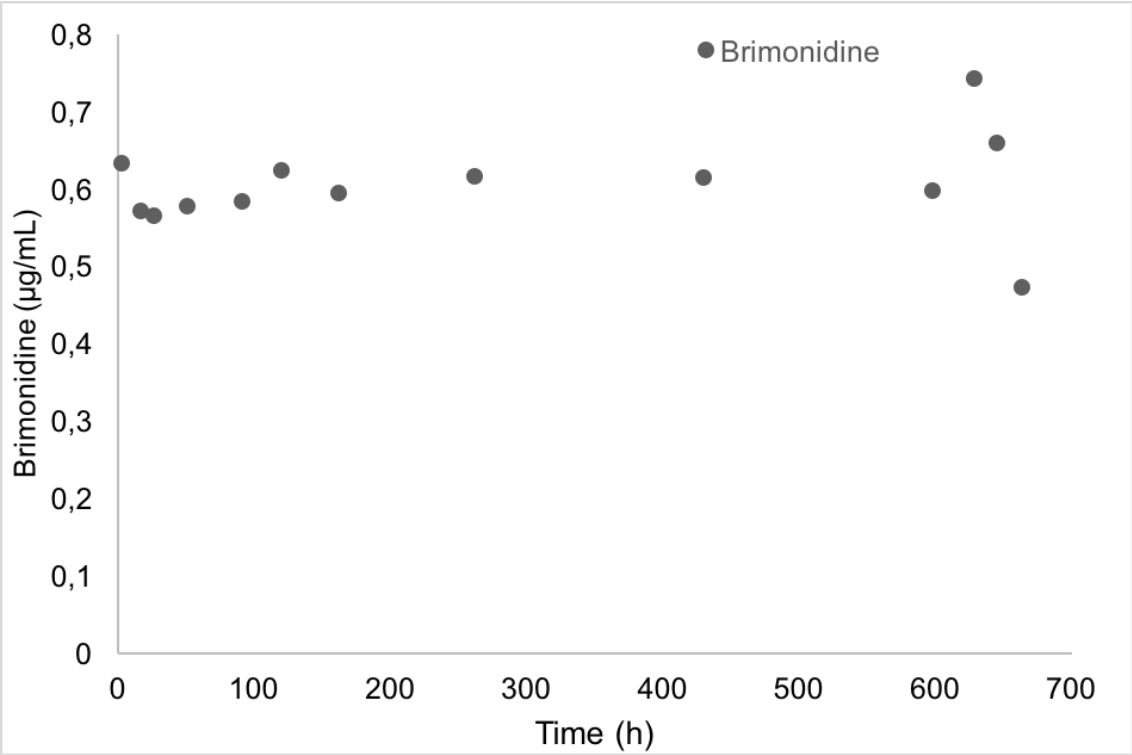

Figure 28 - Concentration of brimonidine released to the PBS solution, obtained from HPLC, from a film composed of eleven groups of (PBAE/GO^{+}/GO^{-}/HP-ß-CD+Brim) as a function of the immersion time.

The film that was immersed in the PBS solution were also analyzed by UV-Vis spectroscopy to quantify the number of layers that remained in the film. This analysis was however influenced by the salts from the PBS solution which deposited in the film surface. The salts deposition caused scattering effects in the spectra, causing the increase in spectrum intensity; the salts lead to light dispersion that reduces the light transmission and appears as absorption. This salt accumulation was visible even by naked eye. For this reason, only a few spectra were considered and compared with the spectra before the film immersion (more spectra are shown in appendix on figure 47).

From figure 29 it is possible to observe that the maximum of the spectrum of the film after 3 hours of immersion in the PBS solution is coincident with that of the spectrum of the film with $(PBAE/GO^{+}/GO^{-})_{11}$ layers before immersion. This result suggests that the HP-ß-CD+Brim layer was released to the PBS solution and that after 3 hours the film keeps its 11 group layers.

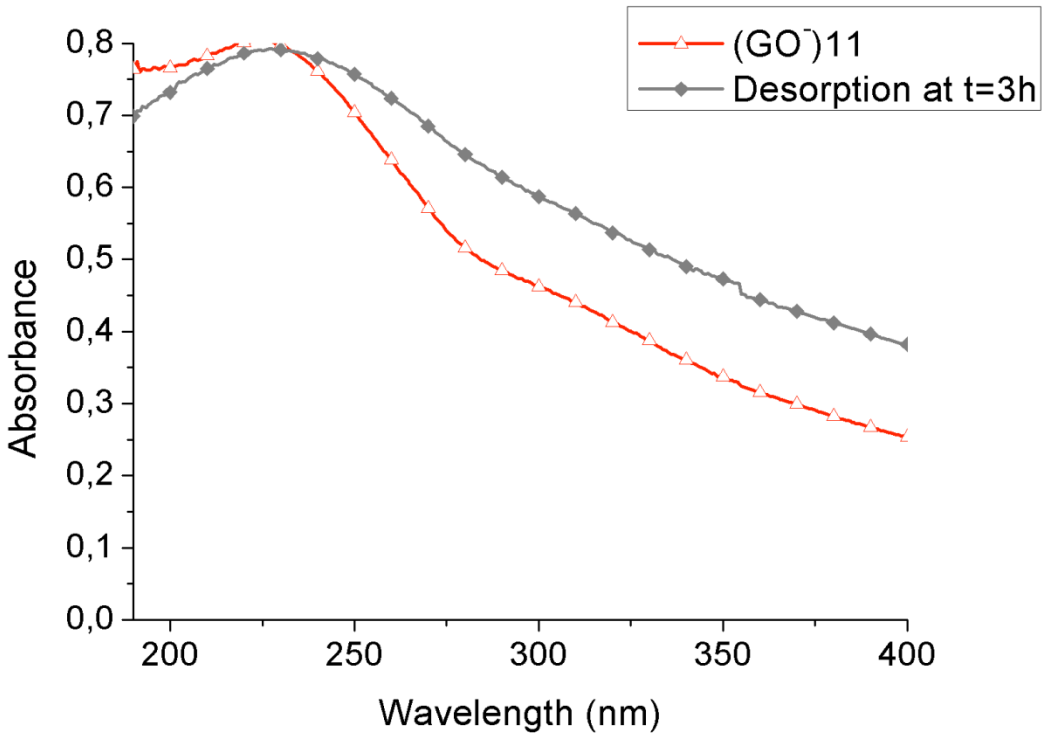

Figure 29 - Spectra of film after 3h min of immersion and spectra of film before immersion with $(PBAE/GO^{+}/GO^{-})_{11}$

According with the other spectra, plotted in figure 30, between the beginning of desorption and 50.75 hours later, the group of layers 11, 10 and 9 were desorbed and the film keeps eight groups of layers ($PBAE/GO^{+}/GO^{-}$/HP-ß-CD+Brim). At this time, the spectrum of the film with the 8^{th} layer of HP-ß-CD+Brim is similar to that of the same film after 50.75 hours of immersion. Also, the 7^{th} layer of GO^{+} represented by the blue line is similar to the spectrum of the film after 88.25 hours of immersion.

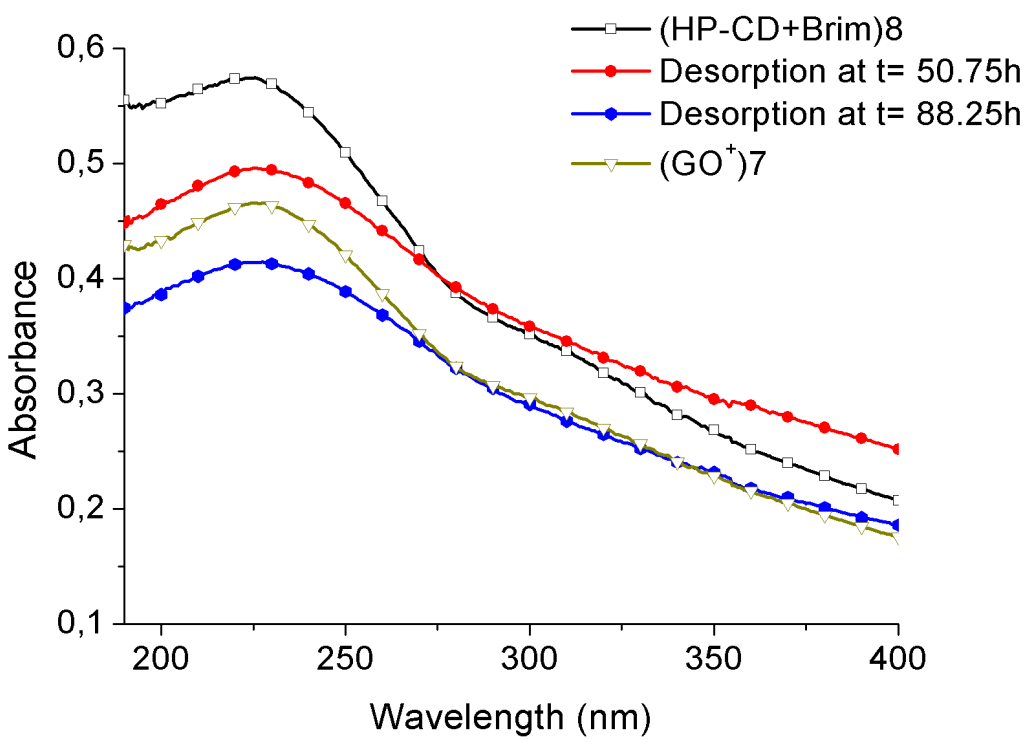

Figure 30 - Spectra of a film after 50.75 h and 88.25 h of immersion and comparison with the spectra films before immersion with $(PBAE/GO^{+})_{7}$ and $(PBAE/GO^{+}/GO^{-}/HP\text{-}ß\text{-}CD+Brim)_{8}$ structures.

After 162.25 hours of immersion, the film has a spectrum that is coincident with that of the 6th layer of HP-ß-CD+Brim, as shown in figure 31. The monitorization of kinetics continued for more than 25 days (t= 621.75 hours) for which it was possible to observe that the spectrum at 621.75 hours is coincident with the spectrum of the 5th layer of HP-ß-CD+Brim, i.e. the $(PBAE/GO^{+}/GO^{-})_{6}$ was desorbed from the film (see figure 32). After 644.75 hours of immersion, it can be concluded that the $(PBAE/GO^{+}/GO^{-})_{5}/(PBAE/GO^{+}/GO^{-})_{4}$ were desorbed from the film and the substrate is on the 3rd layer of the complex HP-ß-CD+Brim since the spectrum obtained at this moment is almost coincident with the spectrum of the 3rd layer of HP-ß-CD+Brim.

Almost 28 days after the beginning of the desorption study, all GO layers were desorbed; the spectrum acquired is coincident with the spectrum obtained for the film with the 1st layer of HP-ß-CD+Brim.

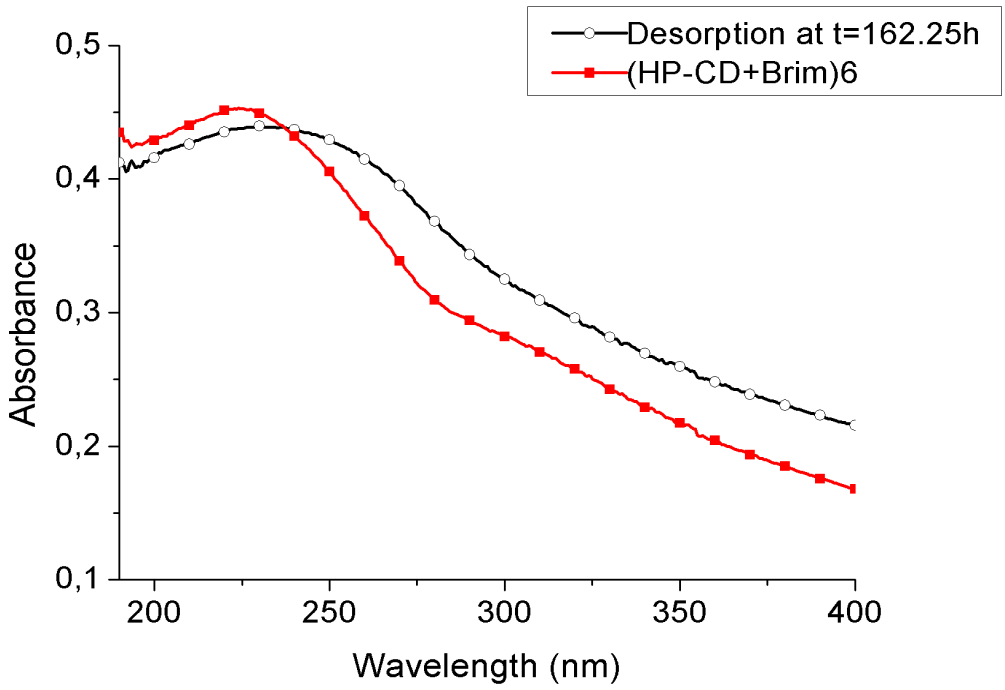

Figure 31 - Spectra of the film after 162.25 h of immersion and of the film before immersion and with $(PBAE/GO^{+}/GO^{-}/HP\text{-}ß\text{-}CD+Brim)_6$ structure.

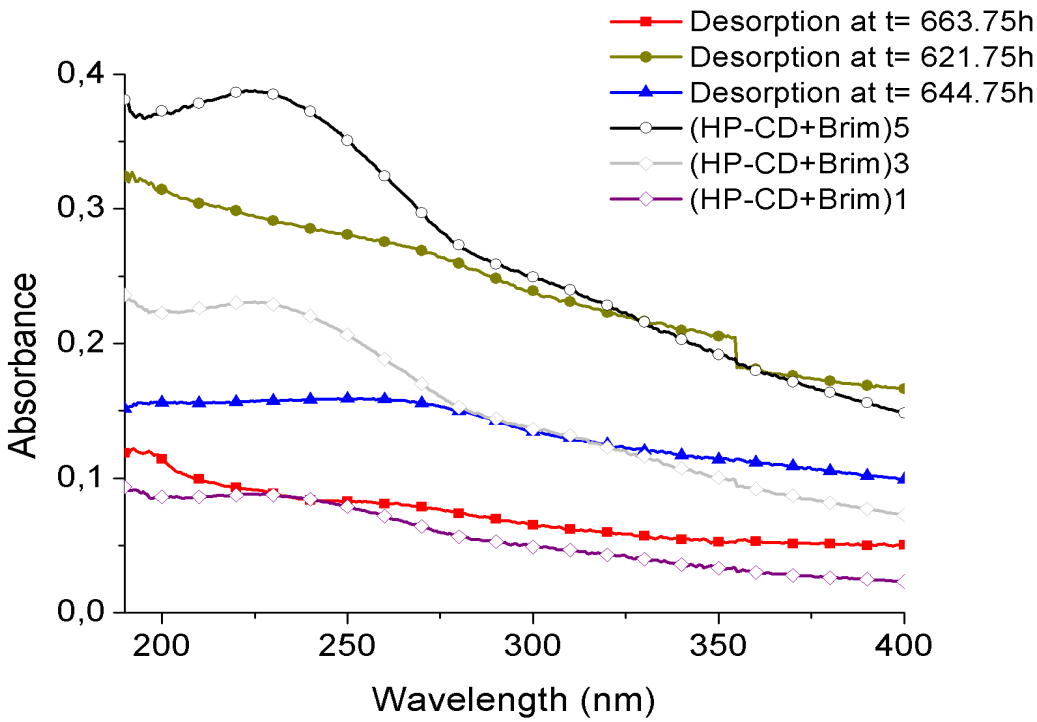

Figure 32 - Spectra of the film after 621.75h, 644.75h and 663.75h of immersion and spectra of films before immersion with $(PBAE/GO^{+}/GO^{-}/HP\text{-}ß\text{-}CD+Brim)_5$, $(PBAE/GO^{+}/GO^{-}/HP\text{-}ß\text{-}CD+Brim)_3$, $(PBAE/GO^{+}/GO^{-}/HP\text{-}ß\text{-}CD+Brim)_1$ structure.

Figure 33 depicts the brimonidine release and the progressive dessorption of all layers. Each blue circle represents the layers that remained in the film at a determined time (t).

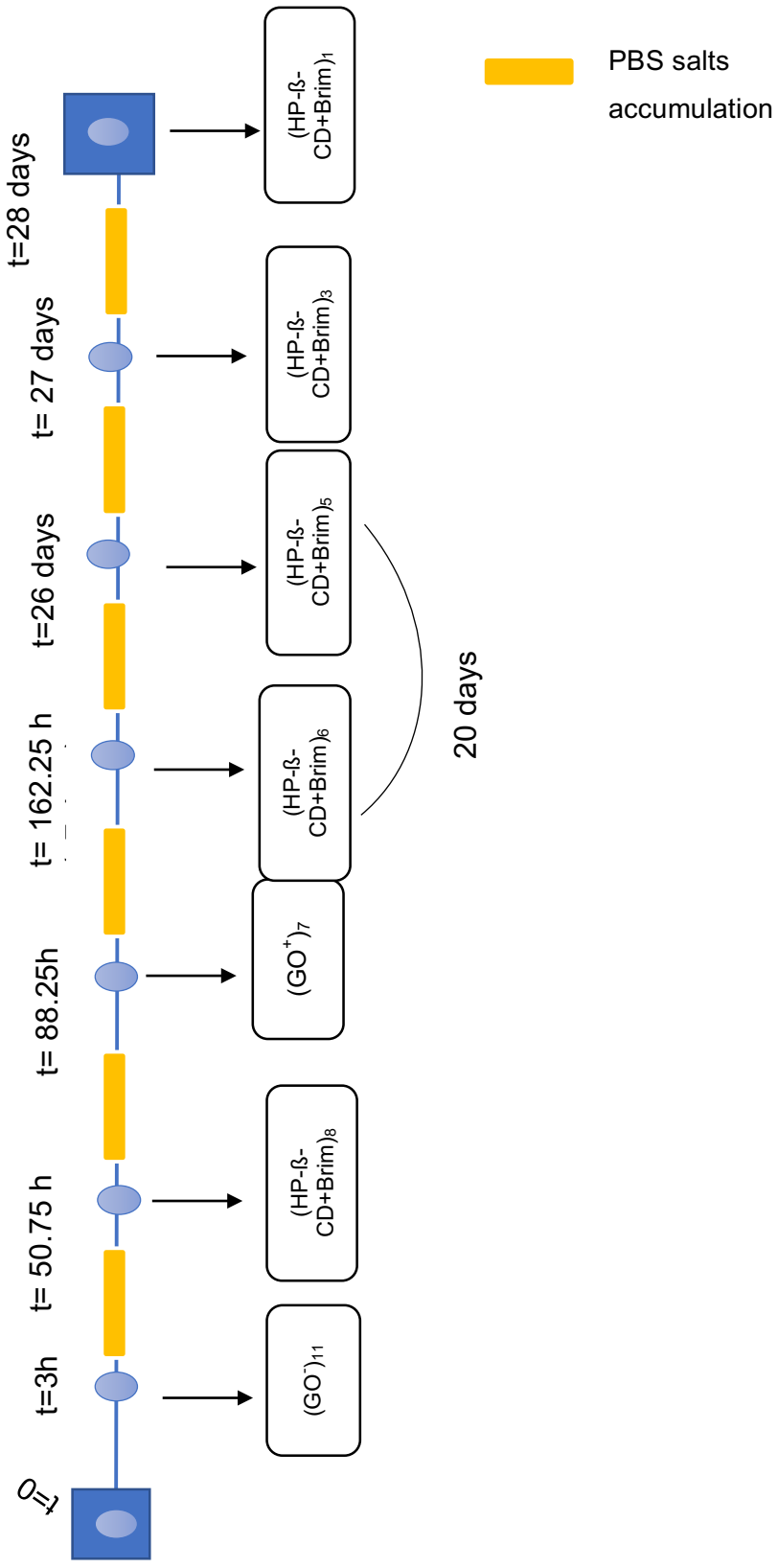

Figure 33 - Schematic representation of brimonidine release kinetics with the evolution of the remaining layers in the film after immersion in the PBS solution

4.2 Brimonidine release kinetics of films with GO^-/GO^+

In order to evaluate the interaction between the graphene charges and brimonidine surface, a film with inverted graphene charges was made. Hence, a film composed of eleven groups of (PBAE/GO^-/GO^+/HP-ß-CD+Brim) was immersed in a PBS solution to follow the brimonidine kinetic release.

Similarly, to the previous studies, this film was also monitorized by UV-Vis spectroscopy and the spectra were compared with those obtained during the film growth. In order to compare with the film described in previous section where the charged layers were inverted (GO^+/GO^-). In this study salt accumulation was visible even by naked eye. For this reason, only a few spectra were considered and compared with the spectra before the film immersion (more spectra are shown in appendix on figure 48).

The drug release monitoring followed the same method, by immersing the film during small periods until a total immersion time of about 30 days. From the results (Figure 34) it can be concluded that between the beginning of the experiment and 2 hours and 25 minutes of immersion time, the 11^{th} group (PBAE/GO^-/GO^+/HP-ß-CD+Brim) was desorbed from the substrate, since the spectrum of the film after 2 hours and 25 minutes of immersion is similar to the spectrum of the film with 10 groups of (PBAE/GO^-/GO^+/HP-ß-CD+Brim).

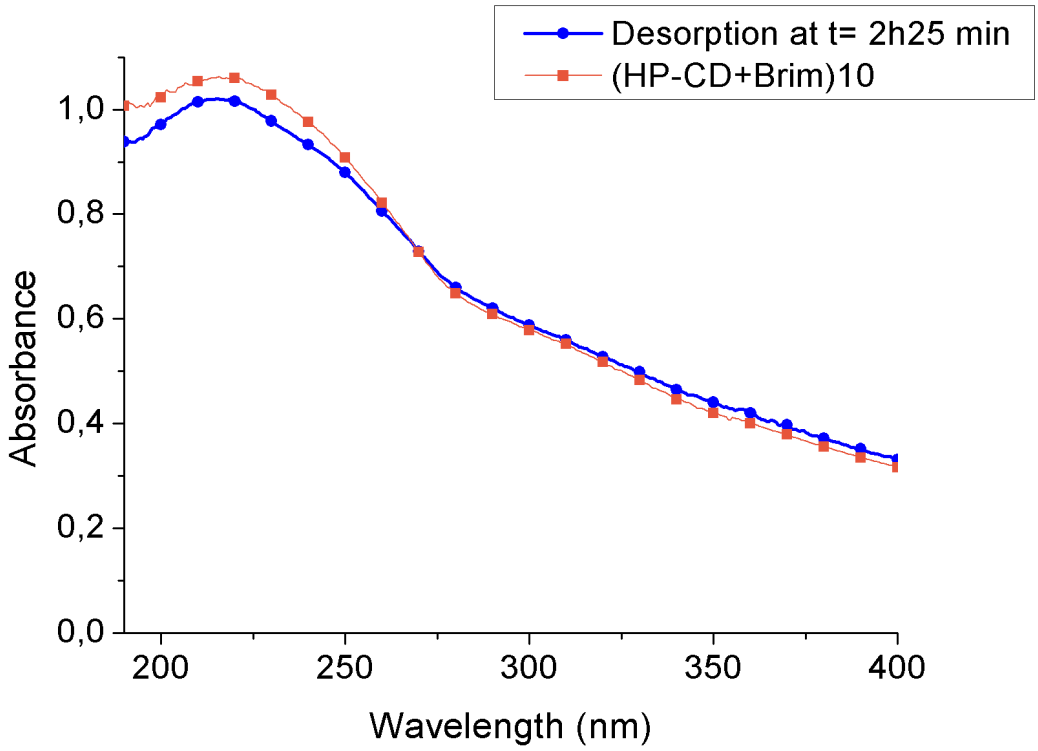

Figure 34 - Spectrum of the film after 2h25 min of immersion and spectrum of a film before immersion with $(PBAE/GO^{-}/GO^{+}/HP\text{-}ß\text{-}CD+Brim)_{10}$ structure.

As shown in figure 35, after 16 hours of immersion time, the spectrum recorded for the film is coincident to the spectrum of the film with $(GO^{+})_8$ layers. In conclusion, after 16 hours of immersion in PBS solution, all the layers in the 10^{th} $(PBAE/GO^{-}/GO^{+}/HP\text{-}ß\text{-}CD+Brim)$ were desorbed, and the 9^{th} layer of HP-ß-CD+Brim was also desorbed from the film.

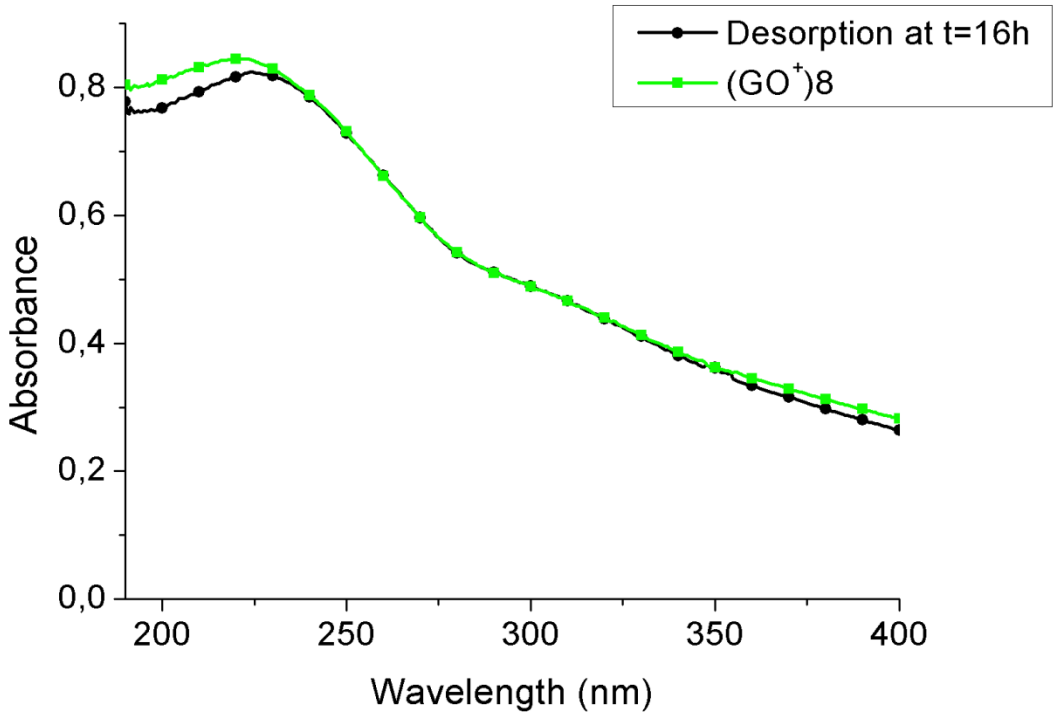

Figure 35 - Comparison between the absorption spectra of film with (PBAE/GO^-/GO^+/HP-ß-CD+Brim)$_8$ layers and after PBS immersion during 16h.

As it may be concluded from figure 36, after 23 hours of immersion time, the layers of 8th and 9th groups desorbed from the film, since the spectrum of the film obtained after 23 hours of immersion in PBS is similar to that obtained for the film with the 7th layer of HP-ß-CD+Brim.

The following layer of HP-ß-CD+Brim was released to the solution after 3h45 min, as it is indicated in the graphic. The monitorization of the release continued during more than 2 days (54h54min). Figure 36 shows that spectrum obtained after this time of immersion is coincident with that obtained for the film with a 7th layer of GO negatively charged.

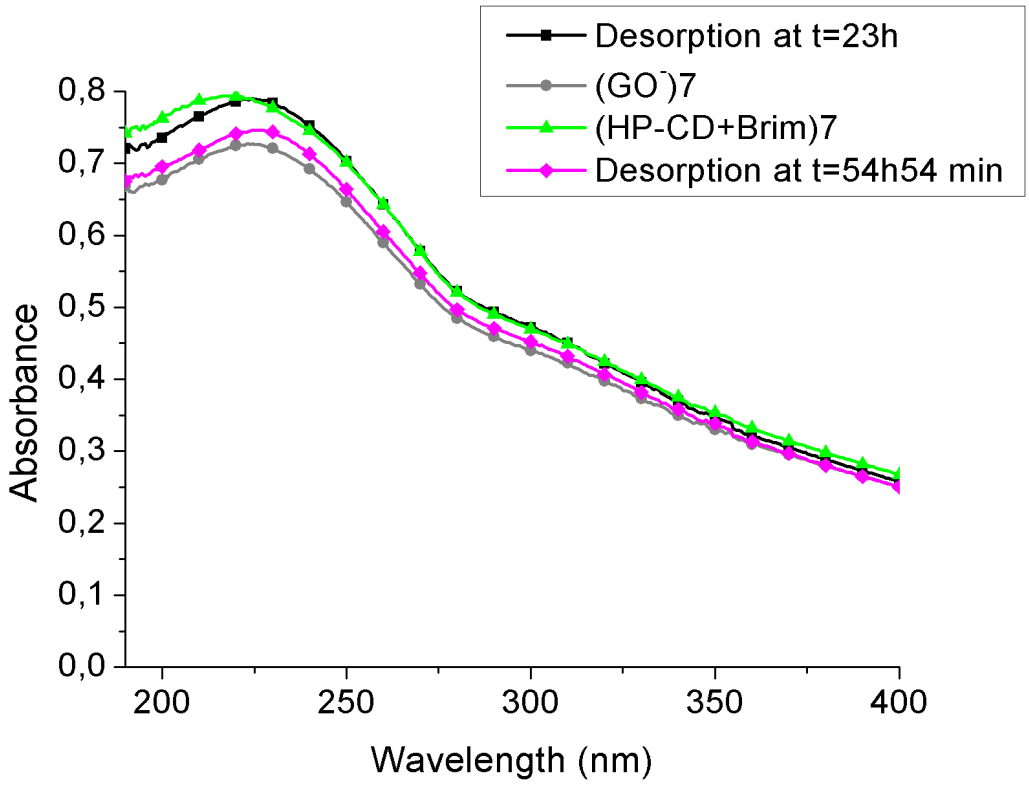

Figure 36 - Spectrum of film after 23h; 54h54 min of immersion and spectrum of film before immersion with the $(PBAE/GO^{-}/GO^{+}/HP\text{-}ß\text{-}CD+Brim)_7$ structure.

Figure 37 shows the spectrum of the film immersed in PBS during more than 16 days (total of 393 hours of immersion time). This spectrum is coincident with the spectrum of the 6th layer of GO^{+}, meaning that the 6th layer of HP-ß-CD+Brim was totally desorbed from the film at this stage. By analyzing figure 38, it can be concluded that after almost 25 days of immersion time (595 hours) the 6th $(PBAE/GO^{-}/GO^{+}/HP\text{-}ß\text{-}CD+Brim)$ group were desorbed from the film, since the spectrum obtained at this time has almost the same maximum intensity as the spectrum of the film with 4 groups of $(PBAE/GO^{-}/GO^{+}/HP\text{-}ß\text{-}CD+Brim)$ and terminating in $(PBAE/GO^{-})$, indicating that GO^{+} and HP-ß-CD+Brim in the 5th layers were desorbed from the film.

To conclude the monitorization of the brimonidine kinetics release, at 763 hours of immersion time (more than 1 month) the spectrum obtained is coincident with the spectrum of the film with 3 layers of HP-ß-CD+Brim, indicating that the group $(PBAE/GO^{-}/GO^{+}/HP\text{-}ß\text{-}CD+Brim)_5/PBAE/GO^{-}/GO^{+}/HP\text{-}ß\text{-}CD+Brim)_4$ were desorbed from the film. The monitorization was stopped at this stage, because after, the spectra showed only noise and could not be compared with the spectra of the films during growth. From these results, it could be concluded that after 30 days all layers of the film were desorbed.

By comparing this film desorption with that of the film described previously on section 3.2 (see figure 22b for film composition), it is found that the brimonidine desorption follows a similar behavior, although the complete release of all the layers of brimonidine and the GO is longer.

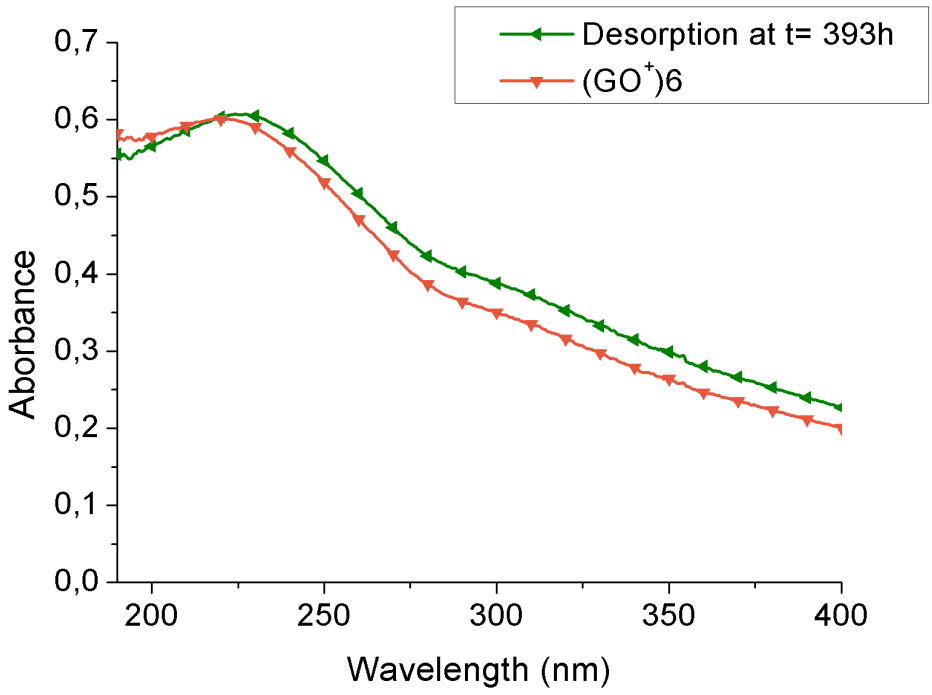

Figure 37 - Spectrum of film after 393h of immersion and spectrum of film before immersion with $(PBAE/GO^{-}/GO^{+}/HP\text{-}ß\text{-}CD+Brim)_6$.

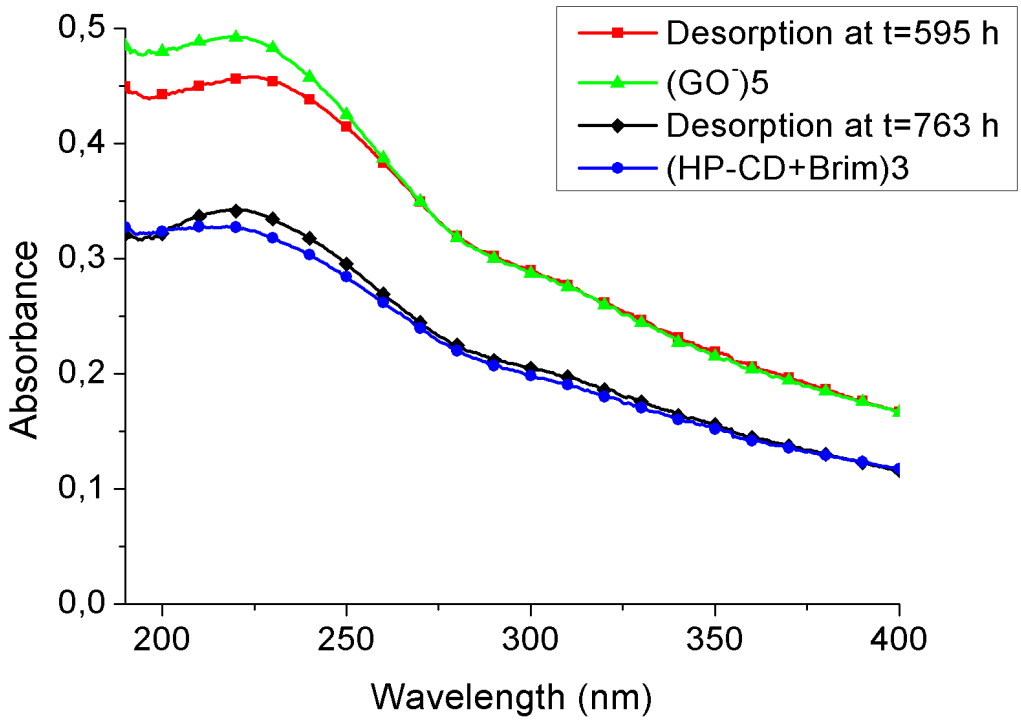

Figure 38 - Spectra of film after 595h and 763h of immersion and spectra of film before immersion with $(PBAE/GO^-/GO^+/HP\text{-}ß\text{-}CD+Brim)_5$/ $PBAE/GO^-/GO^+/HP\text{-}ß\text{-}CD+Brim)_3$.

Figure 39 summarizes the changes in the film composition with the immersion time. Each blue circle represents the layers that remained in the film at a determined time (t).

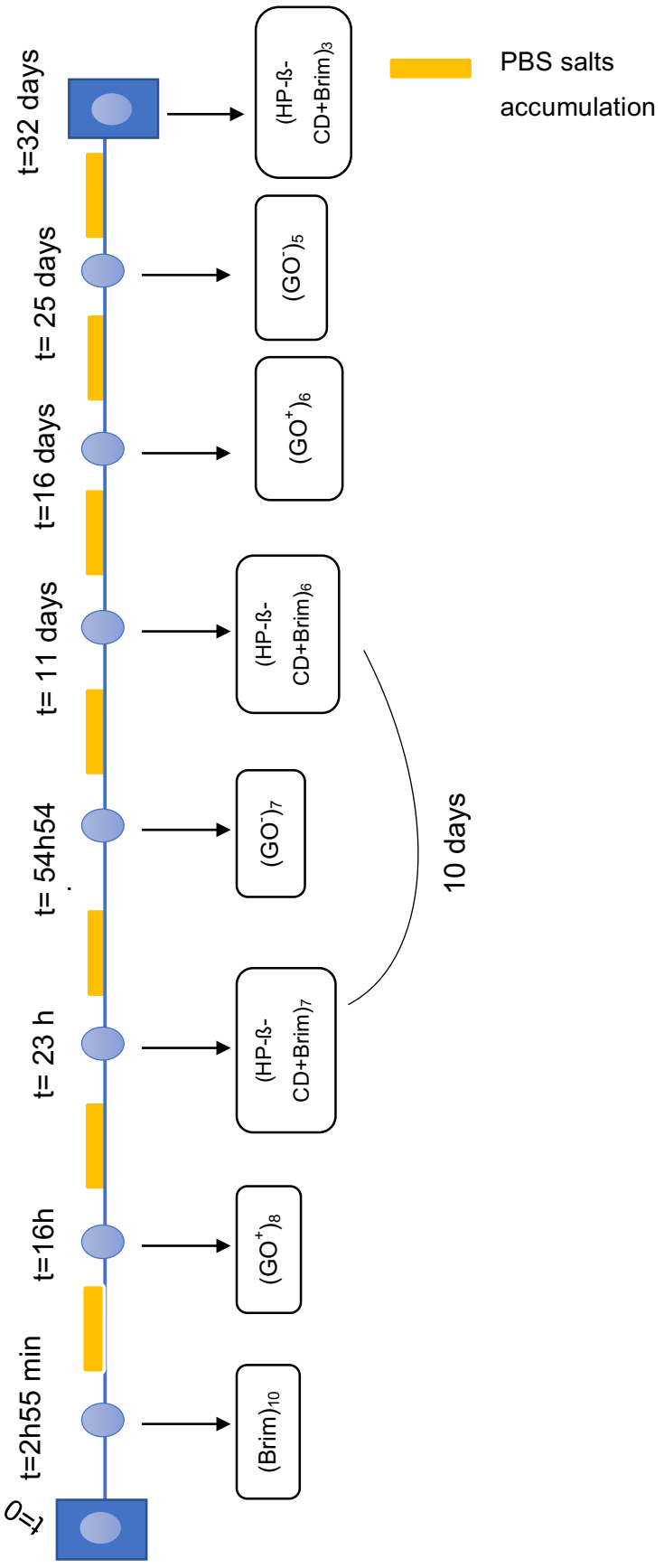

Figure 39 – Schematic representation of brimonidine release kinetics with the evolution of the remaining layers in the film after immersion in the PBS solution.

4.3 Brimonidine release kinetics of films without PBAE

The results obtained for the brimonidine release from the film without PBAE (see figure 22c) were not coherent with a continuous decrease in brimonidine layers. One hypothesis to explain this is that the absence of PBAE allows the interdifusion of consecutive layers thereby causing a disorder in the brimonidine release.

Also, after almost 28 days of immersion, the absorption spectrum was coincident with that of the film with 11 groups containing HP-ß-CD+Brim. For this reason, the desorption study was interrupted and it was concluded the PBAE polymer layer is necessary to efficiently release the graphene and brimonidine layers.

4.4 Brimonidine release kinetics conclusion

From these brimonidine release studies, some conclusions can be drawn that can be useful to improve films architecture in future works. One refers to the charge of the GO surface that seems not to influence the brimonidine release, in terms of total time of drug release. However, small differences between the films morphology were detected and should be considered if the films architecture is to be improved. Also, the behavior of the films during the first three hours of immersion is very different. The film with GO^+/GO^- groups takes about 20 days to release the layers (PBAE/GO^+/GO^-/HP-ß-CD+Brim), while the film with GO^-/GO^+ takes about 10 days to release the same layers. These results suggest that the chemical interaction between the negative graphene surface and the brimonidine is stronger compared with the positive one, to test these interactions it could be performed several tests as use XPS technique, to study the layer thickness AFM, ellipsometry and profilometry should be used in the future.

These results can be interpreted taking into consideration that the chemical interaction between the deprotonated carboxylic groups in negative GO and the brimonidine secondary amine (-NH) groups should be stronger than the interaction between the amine groups of positive GO and the terciary amine groups of brimonidine. Despite this difference, the films with the same number of layers show approximately the same time of drug release. This result can however be masked by the presence of salts in both films and during all the release. Indeed, the salts deposition prevent a more accurate analysis of the film and of the PBS solution. Nevertheless, it was evident that the presence of GO between the DD layers delay the brimonidine release. Previous

results showed that films without GO and with 10 bilayers of (PBAE/Brim) need only few minutes to be degraded (53) therefore providing a very fast and undesirable brimonidine release.

Chapter 5 – Conclusion

5. Conclusions

In this thesis, a new drug delivery system that can potentially be used in glaucoma treatment was developed and investigated. The system consisted of a multilayer film composed of DD layers carrying a drug which is commonly used in ocular diseases – brimonidine – encapsulated in 2-hydroxypropyl-ß-cycloextrin and layers of PBAE and GO to obtain a delay in drug release. The DD films were fabricated by the LbL technique and the growth of films was monitorized by UV-Vis spectroscopy, AFM and HPLC.

By analyzing the surfaces of PBAE, GO and brimonidine layers by AFM, it was concluded that PBAE surface contains grains which may lead to incomplete surface coverage and affect the film growth. The phase image of the surface of GO^+/GO^- showed contrast which suggest the presence of salts from the washing solution, this assumption is in agreement with the *scattering* effect observed on the UV-Vis spectra of such films. Also, the phase images also suggest that GO layer fully covers the previous PBAE layer, revealing that a good interaction is established between the polymer and GO. The (PBAE/GO^+/GO^-/HP-ß-CD+Brim) layer, although showing a low Rrms value, shows an incomplete coverage by the brimonidine layer as determined by the phase images, this incomplete coverage should be at the origin of spectra overlap occurring for such films.

The results obtained from UV-Vis analysis also demonstrated a continuous and stable films growth for both films architectures, (PBAE/GO^+/GO^-/HP-ß-CD+Brim) and (PBAE/GO^-/GO^+/HP-ß-CD+Brim). This was also evidenced by the topography and phase images obtained from all layers showing relatively homogeneous surfaces. A third DD film, without PBAE (PBAE/GO^+/GO^-/HP-ß-CD+Brim/GO^+/GO^-/HP-ß-CD+Brim), was studied and the results showed a less linear growth, thus indicating that in the absence of PBAE interdifusion of consecutive layers should occur and thereby increase disorder in the film growth.

The brimonidine release kinetics was followed by UV-Vis absorption and HPLC by immersing the films in a Phosphate Buffer Saline (PBS) solution with properties similar to biological fluids, in terms of pH and salts concentration. The polymer PBAE, in the presence of a PBS solution, suffers a fast hydrolysis that contributes for a faster brimonidine release, but the presence GO between the DD layers delays the brimonidine release.

The film with the GO^+/GO^- group layers presented stronger chemical interactions between the negative graphene surface and the brimonidine comparing with the film with GO^-/GO^+; this is an important result for the study of time-controlled DD where the order of the charged graphene, and also the number of layers, may be adjusted in order to delay consecutive amounts of drug. However, the alternated GO layers, in both cases, i.e. irrespective to the charge order, are able to delay the brimonidine release, the results obtained from the HPLC analysis and their comparison with those obtained from UV-Vis analysis allowed to establish a kinetics for the drug release in films where intercalated PBAE was used. An important limitation of this study was the occurrence, during the drug release analysis, of accumulation of salts on the top of the films. This influenced the spectroscopy measurements and prevented the analysis of the drug release kinetics over the entire period of time.

In conclusion, this work contributed to the development of new DD films and some important conclusions could be drawn about the how the internal structure of the films and composition can influence he films performance when delivering the drug. Nevertheless, more experiments are required concerning the corroboration of the obtained data, mainly with respect to the desorption studies in order to more precisely understand the drug release kinetics.

Chapter 6 – Future Work

6. Future Work

Although, the results and conclusions obtained in this work allowed to comprehend at a certain level the release behavior of brimonidine as well as the structure of the prepared films, more accurate studies should be performed to better establish those features. In particular, it would be important to monitor in real time the analysis of the PBS solutions, i.e. after each immersion on PBS, the solution should be immediately analyzed by HPLC, because there is no information on the stability of the solutions analyzed.

Regarding the continuation of this study, *in vitro* investigations, should be carried out to determine the adequate dose to be applied *in situ* and better evaluate the potentiality of these films on the glaucoma treatment.

7. Bibliography

1. Davis ME, Brewster ME. Cyclodextrin-based pharmaceutics: past, present and future. Nat Rev Drug Discov. 2004;3:1023–35.
2. Oliveira RRL De, Albuquerque D a. C, Cruz TGS, Leite FMY and FL. Measurement of the Nanoscale Roughness by Atomic Force Microscopy: Basic Principles and Applications. At Force Microsc - Imaging, Meas Manip Surfaces At Scale. 2012;147–74.
3. Marrese M, Guarino V, Ambrosio L. Atomic Force Microscopy: A Powerful Tool to Address Scaffold Design in Tissue Engineering. J Funct Biomater. 2017;8(7):1–20.
4. Champion B. HPLC Separation Fundamentals. Agilent Technologies, Inc.; 2009.
5. Ahmad H, Kronfeldt H. High Sensitive Seawater Resistant SERS Substrates Based on Gold Island Film Produced by Electroless Plating. Mar Sci. 2013;3(1):1–8.
6. Kingman S. Glaucoma is second leading cause of blindness globally. Bull World Health Organ. 2004;82(11):887–8.
7. Gooch N, Molokhia SA, Condie R, Burr RM, Archer B, Ambati BK, et al. Ocular drug delivery for glaucoma management. Pharmaceutics. 2012;4(1):197–211.
8. Cantor LB, Burke J. Brimonidine. Expert Opin Investig Drugs. 1997;6(8):1063–83.
9. Kwon YH, Fingert JH, Kuehn MH, Alward WL. Primary open-angle glaucoma. N Engl J Med. 2009;360(11):1113–24.
10. Goldberg LD. Disease management programs for glaucoma - Has the vision become a reality? Dis Manag Heal Outcomes. 2007;15(4):199–205.
11. Casson RJ, Chidlow G, Wood JPM, Crowston JG, Goldberg I. Definition of glaucoma: Clinical and experimental concepts. Clin Exp Ophthalmol. 2012;40(4):341–9.
12. Wójcik-Gryciuk A, Skup M, Waleszczyk WJ. Glaucoma -state of the art and perspectives on treatment. Restor Neurol Neurosci. 2015;34(1):107–23.
13. Lavik E, Kuehn MH, Kwon YH. Novel drug delivery systems for glaucoma. Eye (Lond). 2011;25(5):578–86.
14. Infeld DA, Shea JGO. concepts Glaucoma : diagnosis and management. 1998;(June):709–15.
15. Jain KK. Drug delivery systems - an overview. Methods Mol Biol. 2008;437:1–50.
16. Pharmaceutics: Drug Delivery and Targeting. 2nd Ed. Fasttrack; 2012.
17. Jinkee Hong, Nisarg J. Shah, Adam C. Drake, Peter C. DeMuth, Jong Bum Lee,

Jianzhy Chen and Paula T. Hammond. Graphene Multilayers as Gates for Multi-Week Sequential Release of Proteins from Surfaces. 2012;(1):81–8.

18. Keeney M, Jiang XY, Yamane M, Lee M, Goodman S, Yang F. Nanocoating for biomolecule delivery using layer-by-layer self-assembly. J Mater Chem B. 2015;3(45):8757–8770.
19. Decher G, Hong JD, Schmitt J. Buildup of ultrathin multilayer films by a self-assembly process: III. Consecutively alternating adsorption of anionic and cationic polyelectrolytes on charged surfaces. Thin Solid Films. 1992;210–211:831–5.
20. Richardson JJ, Bjornmalm M, Caruso F. Technology-driven layer-by-layer assembly of nanofilms. Science (80-). 2015;348(6233):aaa2491-aaa2491.
21. Gentile P, Carmagnola I, Nardo T, Chiono V. Layer-by-layer assembly for biomedical applications in the last decade. Nanotechnology. 2015;26:1–21.
22. Piotrowski G, Butler JH, Richardson DC. Preclinical evaluation of brimonidine. Surv Ophthalmol. 1996;41(1):S9–18.
23. H S, Li Y, Fan X, Zhang F, Zhang G. β-Cyclodextrin Functionalized Graphene Oxide: an Efficient and Recyclable Adsorbent for the Removal of Dye Pollutants. Front Chem Sci Eng. 2015;9(1):77–83.
24. Mahmoud KA, Mansoor B, Mansour A, Khraisheh M. Functional graphene nanosheets: The next generation membranes for water desalination. Desalination. 2015;356:208–25.
25. Guo Y, Guo S, Ren J, Zhai Y, Dong S, Wang E. Nanosheets with High Supramolecular Recognition Capability Synthesis and Host Guest Inclusion for Enhanced Electrochemical Performance.pdf. 2010;4(7):4001–10.
26. Wang K, Ruan J, Song H, Zhang J, Wo Y, Guo S, et al. Biocompatibility of Graphene Oxide. Nanoscale Res Lett. 2011;6(1):1–8.
27. Lynn DM, Langer R. Degradable Poly (beta-amino esters): Synthesis , Characterization , and Self-Assembly with Plasmid DNA. J Am Chem Soc. 2000;122(10):10761–8.
28. Smith RC. Toward a Drug Delivery Coating for Intraocular. 2010;
29. Deng X, Zheng N, Song Z, Yin L, Cheng J. Trigger-responsive, fast-degradable poly(β-amino ester)s for enhanced DNA unpackaging and reduced toxicity. Biomaterials. 2014;35(18):5006–15.
30. Luten J, van Nostrum CF, De Smedt SC, Hennink WE. Biodegradable polymers as non-viral carriers for plasmid DNA delivery. J Control Release. 2008;126(2):97–110.
31. Green JJ, Langer R, Anderson DG, Luten J, van Nostrum CF, De Smedt SC, et al. Trigger-responsive, fast-degradable poly(β-amino ester)s for enhanced DNA

unpackaging and reduced toxicity. Acc Chem Res. 2008;126(18):5006–15.
32. Duchêne D, Bochot A. Thirty years with cyclodextrins. Int J Pharm. 2016;514(1):58–72.
33. Oliveri V, Vecchio G. Cyclodextrins as protective agents of protein aggregation: An overview. Chem - An Asian J. 2016;11(11):1648–57.
34. Challa R, Ahuja A, Ali J, Khar RK. Cyclodextrins in drug delivery: an updated review. AAPS PharmSciTech. 2005;6(2):E329–57.
35. Baranowski PB, Gajda M, Pluta J. Review Article Ophthalmic Drug Dosage Forms : Characterisation and Research Methods. 2014;2014.
36. Gould S, Scott RC. 2-Hydroxypropyl-β-cyclodextrin (HP-β-CD): A toxicology review. Food Chem Toxicol. 2005;43(10):1451–9.
37. Sleath B, Blalock SJ, Covert D, Skinner AC, Muir KW, Robin AL. Patient race, reported problems in using glaucoma medications, and adherence. ISRN Ophthalmol. 2012;2012:1–7.
38. Offeman WSHJ and RE. Preparation of Graphitic Oxide. Natl Lead Co. 1958;1339.
39. Graphene LA. Highly Tunable Charge Transport in Layer-by-Layer Assembled Graphene Transistors. ACS Nano. 2012;(3):2432–40.
40. Owen T. Principles and Applications of UV-Visible spectroscopy. Fundamentals of UV-visible spectroscopy. Primer; 1996.
41. Mosorov V. The Lambert-Beer law in time domain form and its application. Appl Radiat Isot. 2017;128:1–5.
42. Skoog, Douglas A.; West, Donald M.; Hollar JF. Analytical Chemestry: An Introduction [Internet]. 7th ed. Emily Barrosse; 2000. Available from: http://pubs.acs.org/doi/abs/10.1021/ed069pA305.1
43. Scott WW, Bhushan B. Use of phase imaging in atomic force microscopy for measurement of viscoelastic contrast in polymer nanocomposites and molecularly thick lubricant films. Ultramicroscopy. 2003;97(1–4):151–69.
44. Binnig G, Quate CF. Atomic Force Microscope. Phys Rev Lett. 1986;56(9):930–3.
45. Barattin R, Voyer N. Chemical modifications of AFM tips for the study of molecular recognition events. Chem Commun. 2008;(13):1513–32.
46. Variola F. Atomic force microscopy in biomaterials surface science. Phys Chem Chem Phys. 2015;17:2950–9.
47. Raposo M, Ferreira Q, Ribeiro P a. A Guide for Atomic Force Microscopy Analysis of Soft- Condensed Matter. Mod Res Educ Top Microsc. 2007;758–69.
48. Tognarelli JM, Dawood M, Shariff MIF, Grover VPB, Crossey MME, Cox IJ, et al.

Magnetic Resonance Spectroscopy: Principles and Techniques: Lessons for Clinicians. J Clin Exp Hepatol [Internet]. 2015;5(4):320–8. Available from: http://dx.doi.org/10.1016/j.jceh.2015.10.006

49. Mlynárik V. Introduction to nuclear magnetic resonance. Anal Biochem. 2016;1–6.
50. Depciuch J, Kaznowska E, Zawlik I, Wojnarowska R, Cholewa M, Heraud P, et al. Application of Raman Spectroscopy and Infrared Spectroscopy in the Identification of Breast Cancer. Appl Spectrosc. 2016;70(2):251–63.
51. Medders GR, Paesani F. Infrared and raman spectroscopy of liquid water through “first-principles” many-body molecular dynamics. J Chem Theory Comput. 2015;11(3):1145–54.
52. Lee DW, Hong T-K, Kang D, Lee J, Heo M, Kim JY, et al. Highly controllable transparent and conducting thin films using layer-by-layer assembly of oppositely charged reduced graphene oxides. J Mater Chem. 2011;21(10):3438.
53. Mónica Sofia da Costa Araújo. Tese de Mestrado. Nanostructured films for controlled release of drugs for glaucoma treatment. Instituto Superior Técnico; 2016.
54. Lloyd R. Snyder, Joseph J.Kirkland JWD. Introduction to Modern Liquid Chromatography, Third Edition. 3rd Ed. Wiley, editor. Journal of The American Society for Mass Spectrometry. 2010.
55. Jorge TFP. Nutrientes e suplementos nutricionais em vegetais e frutos frequentemente usados na dieta: Estudo por espectrometria de massa do resveratrol. Faculdade de Ciências; 2012.
56. Skoog D. A., Holler F. j. CSR. Principles of Instrumental Analysis. 6th Ed. Thomson Brooks/Cole, editor. 2007.
57. Elshanawane, Abdullah A, Lobna M Abdelaziz MSM and HMH. Development and Validation of HPLC Method for Simultaneous Estimation of Brimonidine Tartrate and Timolol Maleate in Bulk and Pharmaceutical Dosage Form. J Chromatogr Sep Tech. 2014;5(3):1–5.
58. Mcintire TM, Smalley SR, Newberg JT, Lea S, Hemminger JC, Finlayson-pitts BJ, et al. Substrate Changes Associated with the Chemistry of Self-Assembled Monolayers on Silicon Substrate Changes Associated with the Chemistry of Self-Assembled Monolayers on Silicon. Society. 2006;(16):5617–24.
59. Neupane GP, Dhakal KP, Kim MS, Lee H, Guthold M, Joseph VS, et al. Simple method of DNA stretching on glass substrate for fluorescence imaging and spectroscopy. J Biomed Opt. 2014;19(5):1–6.
60. Shofner S, Glaucoma N, Month A. Renowned Eye Surgeon Dr . Stewart Shofner

Expresses The Importance of National Glaucoma Awareness Month Dr . Stewart Shofner of Shofner Vision Center in Nashville , TN joins leading eye and health. 2015;2–4.

Appendix

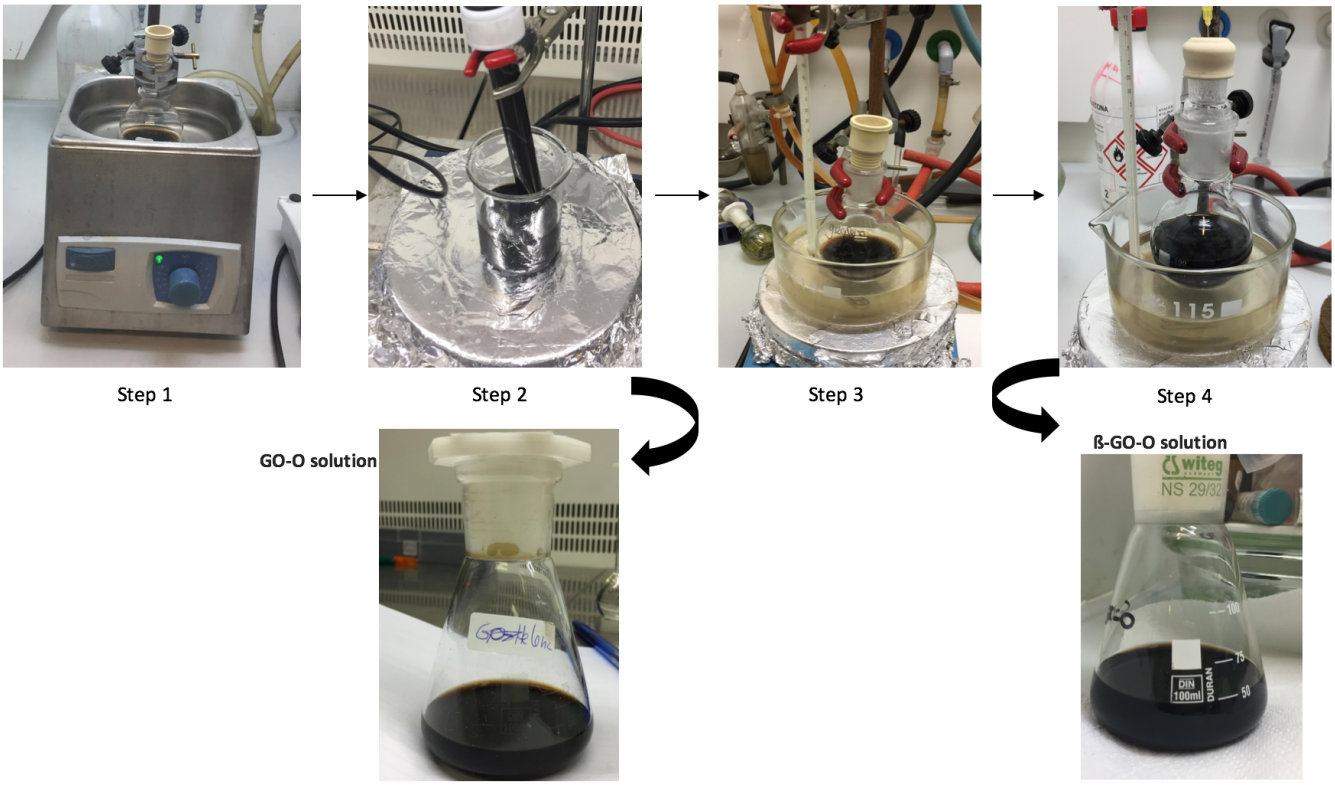

Figure 40 - Steps involved in the synthesis carried out to obtain GO-ß-CD from GO.

Figure 41 - UV-Vis Cecil Aquarius CE7200 spectrophotometer.

Figure 42 - Nano-Observer AFM from CSInstruments.

Figure 43 - Oxygen Plasma Chamber, Gala Instrumente Plasma Prep 2.

Figure 44 - HPLC system – Elite LaChrom.

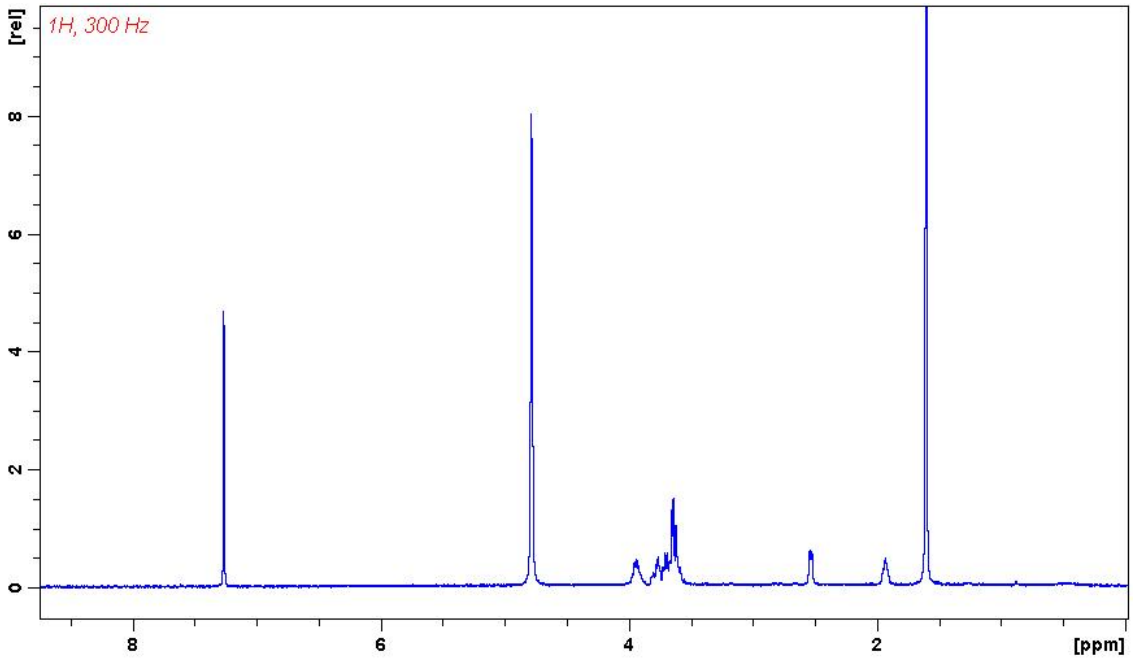

Figure 45 – 1H-NMR spectrum of dried GO-O in D_2O.

Table 5 - AFM images of the prepared films with different structures, scan size 2 µm.

PBAE – Scan size 2 µm		
Topography	Phase	Profile line
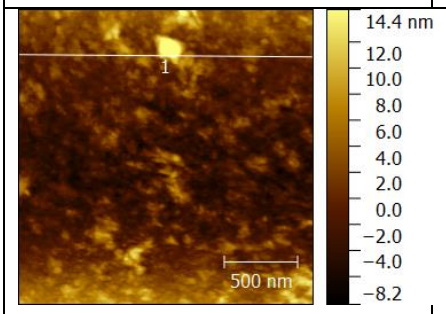	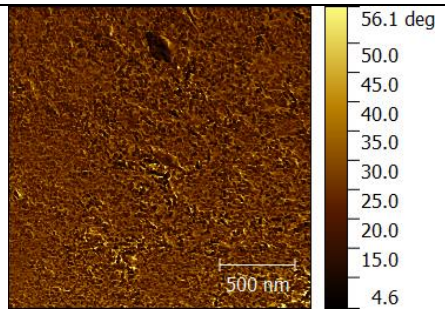	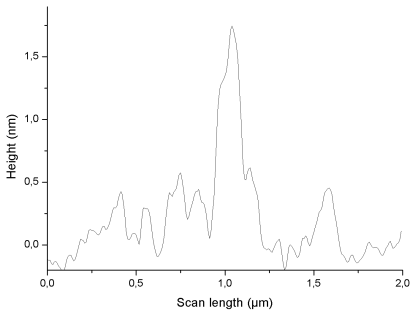
PBAE/GO^{+}/GO^{-} – Scan size 2 µm		
Topography	Phase	Profile line
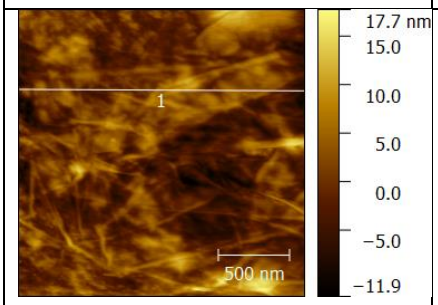	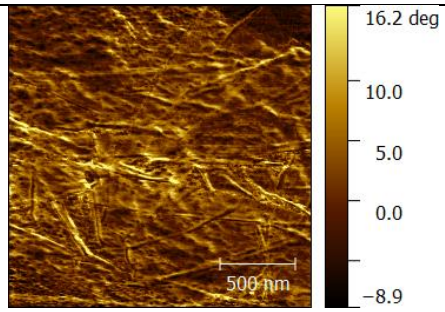	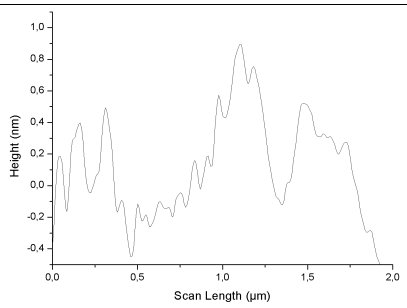
PBAE/GO^{+}/GO^{-}/HP-ß-CD+Brim – Scan size 2 µm		
Topography	Phase	Profile line
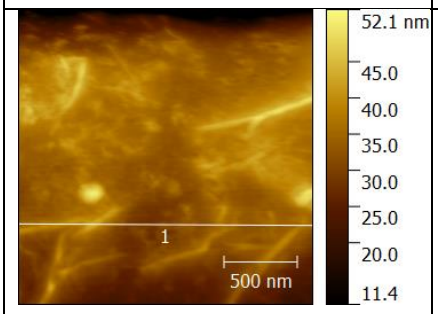	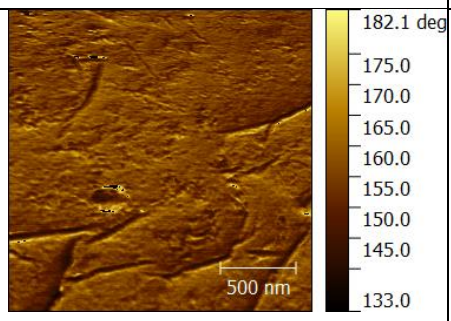	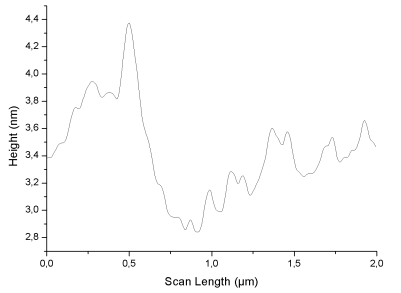

Table 6 - AFM images of the prepared films with different structures, scan size 2 µm.

PBAE/GO$^+$/GO$^-$/HP-ß-CD+Brim/PBAE – Scan size 2 µm		
Topography	Phase	Profile line
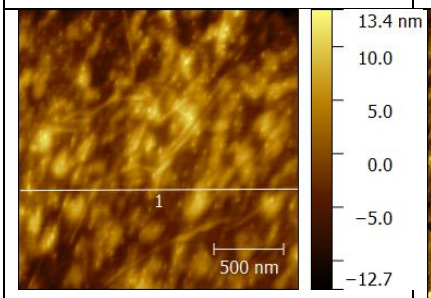	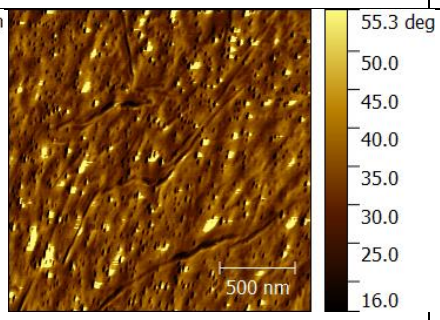	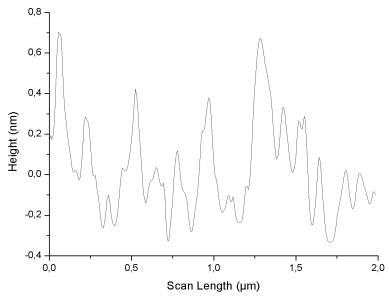
PBAE/GO$^+$/GO$^-$/HP-ß-CD+Brim/PBAE/GO$^+$/GO$^-$ – Scan size 2 µm		
Topography	Phase	Profile line
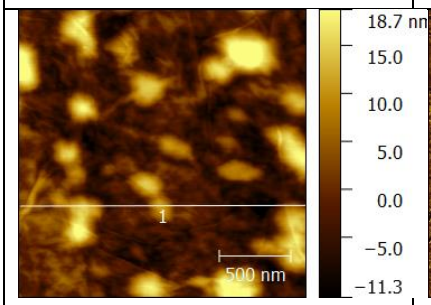	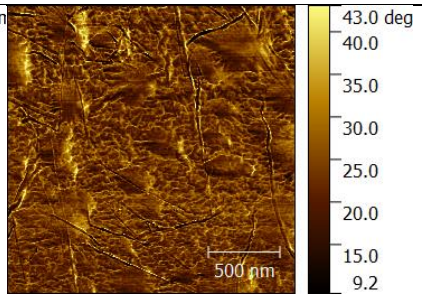	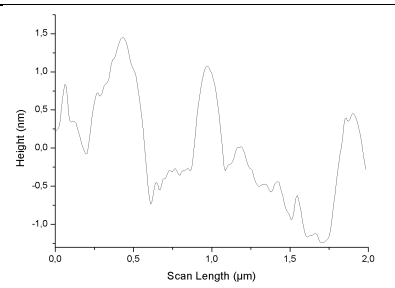
PBAE/GO$^+$/GO$^-$/HP-ß-CD+Brim/GO$^+$/GO$^-$ – Scan size 2 µm		
Topography	Phase	Profile line
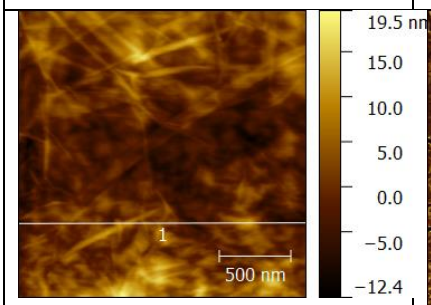	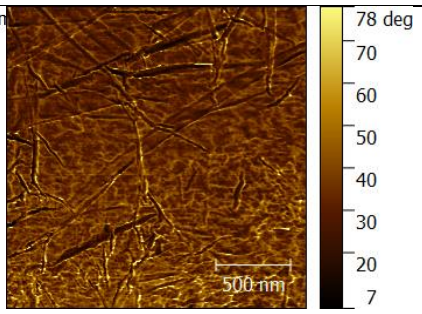	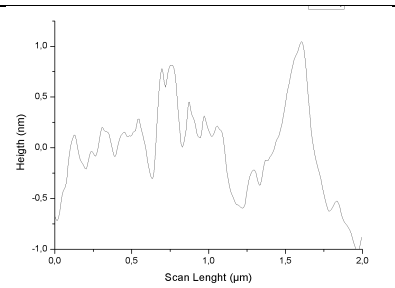

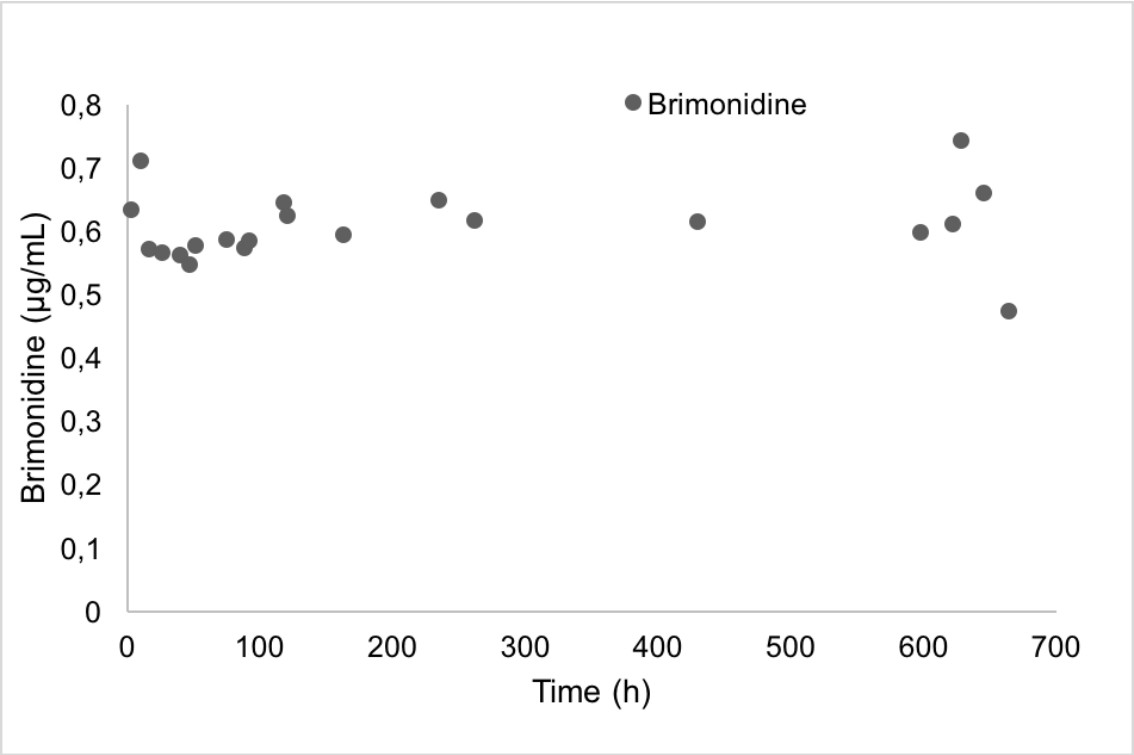

Figure 46 - Concentration of brimonidine obtained from HPLC and released to the PBS solution from a film composed of eleven groups of (PBAE/GO^{+}/GO^{-}/HP-ß-CD+Brim) as a function of the immersion time and obtained.

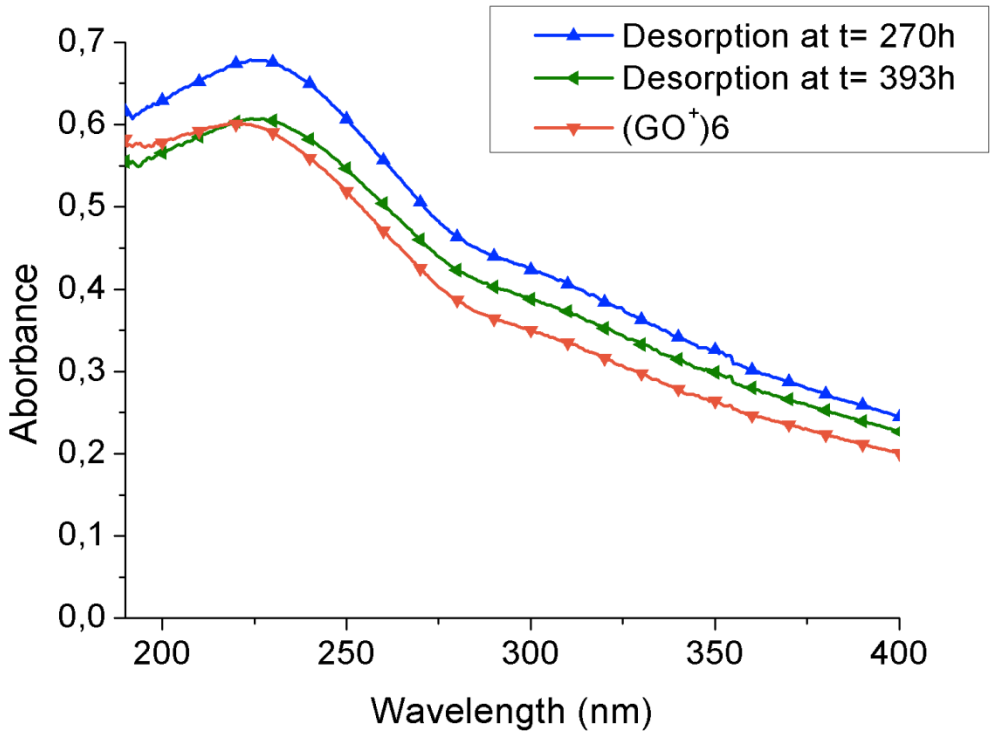

Figure 47 - Spectra of film after 270h and 393 h of immersion and spectra of film before immersion with $(PBAE/GO^{+}/GO^{-}/HP\text{-}ß\text{-}CD+Brim)_{6}$.

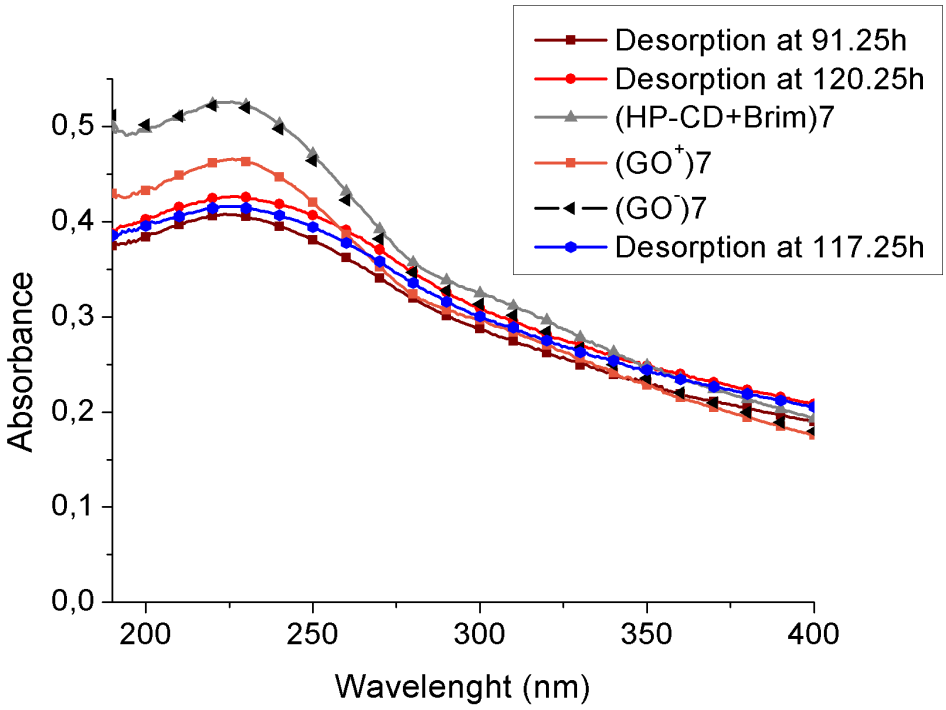

Figure 48 - Spectra of film after 91.25h, 117.25h and 120.25h of immersion and spectra of film before immersion with $(PBAE/GO^{-}/GO^{+}/HP\text{-}ß\text{-}CD+Brim)_{7}$.

Area % Report

Data File: C:\EZChrom Elite\Projects\Instituto Telecomunicações\Data\HPLC-UV.10002 24-06-2017 09-49-33.dat
Method: C:\EZChrom Elite\Projects\Instituto Telecomunicações\Method\Brimonidine_release_BDSHYPERSIL_flow1.0.met
Acquired: 24/06/2017 09:50:46
Printed: 29/06/2017 09:47:51

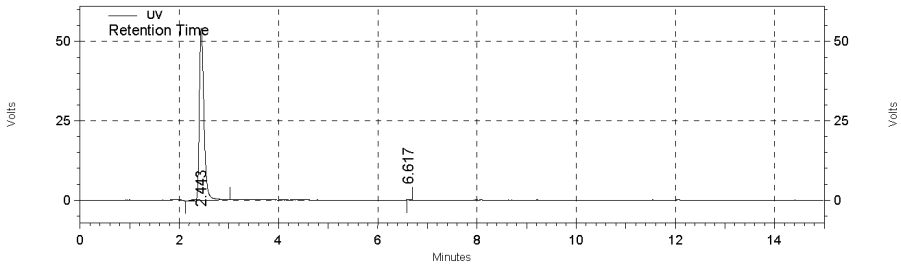

UV Results

Retention Time	Area	Area %	Height	Height %
2.443	1410776	99.97	217508	99.94
6.617	491	0.03	130	0.06
Totals	1411267	100.00	217638	100.00

Figure 49 - Chromatogram obtained from the HPLC software, standard concentration 4 µg/mL of brimonidine.

Area % Report

Data File: C:\EZChrom Elite\Projects\Instituto Telecomunicações\Data\HPLC-UV.10002 24-06-2017 10-05-59.dat
Method: C:\EZChrom Elite\Projects\Instituto Telecomunicações\Method\Brimonidine_release_BDSHYPERSIL_flow1.0.met
Acquired: 24/06/2017 10:07:13
Printed: 29/06/2017 09:46:06

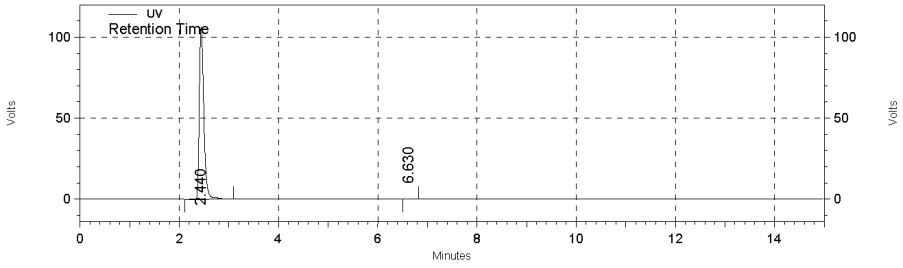

UV Results

Retention Time	Area	Area %	Height	Height %
2.440	2716064	99.87	426205	99.91
6.630	3625	0.13	367	0.09
Totals	2719689	100.00	426572	100.00

Figure 50 - Chromatogram obtained from the HPLC software, standard concentration 10 µg/mL of brimonidine.

Area % Report

Data File: C:\EZChrom Elite\Projects\Instituto Telecomunicações\Data\HPLC-UV.10002 24-06-2017 10-22-24.dat
Method: C:\EZChrom Elite\Projects\Instituto Telecomunicações\Method\Brimonidine_release_BDSHYPERSIL_flow1.0.met
Acquired: 24/06/2017 10:23:37
Printed: 29/06/2017 09:49:08

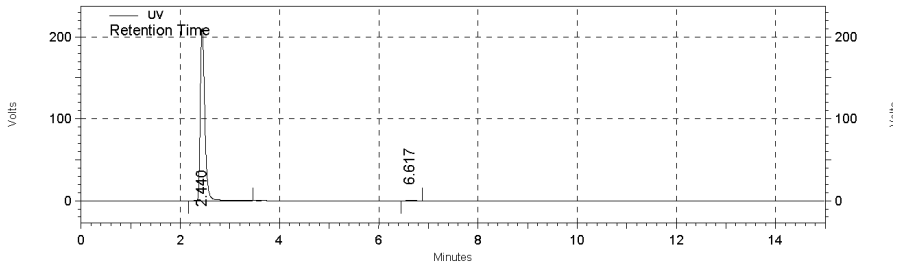

UV Results

Retention Time	Area	Area %	Height	Height %
2.440	5372048	99.82	843830	99.90
6.617	9678	0.18	816	0.10
Totals	5381726	100.00	844646	100.00

Figure 51 - Chromatogram obtained from the HPLC software, standard concentration 15 µg/mL of brimonidine.

Area % Report

Data File: C:\EZChrom Elite\Projects\Instituto Telecomunicações\Data\HPLC-UV.10002 24-06-2017 10-55-13.dat
Method: C:\EZChrom Elite\Projects\Instituto Telecomunicações\Method\Brimonidine_release_BDSHYPERSIL_flow1.0.met
Acquired: 24/06/2017 10:56:27
Printed: 29/06/2017 09:52:38

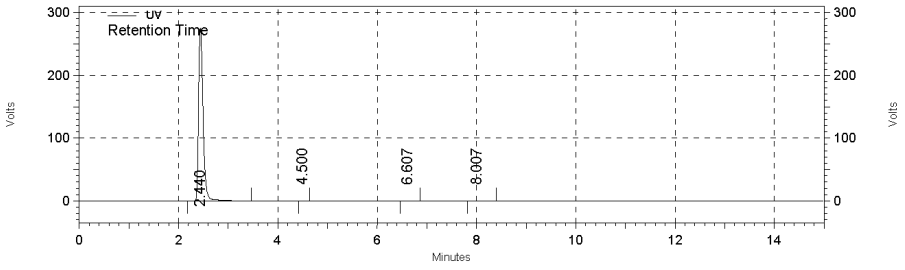

UV Results

Retention Time	Area	Area %	Height	Height %
2.440	6968153	99.72	1101582	99.85
4.500	3057	0.04	451	0.04
6.607	7957	0.11	698	0.06
8.007	8726	0.12	542	0.05
Totals	6987893	100.00	1103273	100.00

Figure 52 - Chromatogram obtained from the HPLC software, standard concentration 20 µg/mL of brimonidine.

Area % Report

Data File: C:\EZChrom Elite\Projects\Instituto Telecomunicações\Data\HPLC-UV.10002 24-06-2017 10-38-45.dat
Method: C:\EZChrom Elite\Projects\Instituto Telecomunicações\Method\Brimonidine_release_BDSHYPERSIL_flow1.0.met
Acquired: 24/06/2017 10:40:01
Printed: 29/06/2017 09:50:30

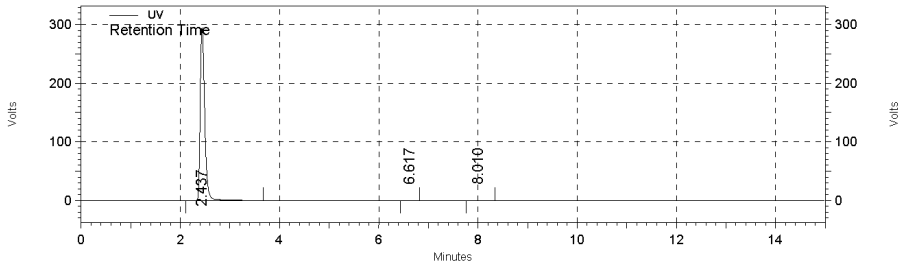

UV Results

Retention Time	Area	Area %	Height	Height %
2.437	7499650	99.71	1179219	99.87
6.617	11267	0.15	994	0.08
8.010	10602	0.14	570	0.05
Totals	7521519	100.00	1180783	100.00

Figure 53 - Chromatogram obtained from the HPLC software, standard concentration 24 µg/mL of brimonidine.